Manuscript <u>≛</u>

Generated using the official AMS LATEX template v6.1

Links between climate sensitivity and the large-scale atmospheric circulation in a simple general circulation model circulation model

Luke L. B. Davis, David W. J. Thompson, and Thomas Birner

Corresponding author: Luke L. B. Davis, lukelbd@colostate.edu

Department of Atmospheric Science, Colorado State University, Fort Collins, USA

Meteorological Institute, Ludwig-Maximilians-University, Munich, Germany

1

Early Online Release: This preliminary version has been accepted for publication in *Journal of Climate* be fully cited, and has been assigned DOI 10.1175/JCLI-D-21-0320.1. The final typeset copyedited article will replace the EOR at the above DOI when it is published.

© 2022 American Meteorological Society

ABSTRACT: Thermodynamical and dynamical aspects of the climate system response to anthropogenic forcing are often considered in two distinct frameworks: The former in the context of the forcing-feedback framework; the latter in the context of eddy-mean flow feedbacks and large-scale thermodynamic constraints. Here we use experiments with the dynamical core of a general circulation model (GCM) to provide insights into the relationships between these two frameworks.

We first demonstrate that the climate feedbacks and climate sensitivity in a dynamical core model are determined by its prescribed thermal relaxation timescales. We then perform two experiments: One that explores the relationships between the thermal relaxation timescale and the climatological circulation; and a second that explores the relationships between the thermal relaxation timescale and the circulation response to a global warming-like forcing perturbation. The results indicate that shorter relaxation timescales (i.e., lower climate sensitivities in the context of a dynamical core model) are associated with 1) a more vigorous large-scale circulation, including increased thermal diffusivity and stronger and more poleward storm tracks and eddy-driven jets and 2) a weaker poleward displacement of the storm tracks and eddy-driven jets in response to the global warming-like forcing perturbation. Interestingly, the circulation response to the forcing perturbation effectively disappears when the thermal relaxation timescales are spatially uniform, suggesting that the circulation response to homogeneous forcing requires spatial inhomogeneities in the local feedback parameter. Implications for anticipating the circulation response to global warming and thermodynamic constraints on the circulation are discussed.

1. Introduction

The forcing-feedback framework is widely used to explore the climate system response to forcing perturbations. The most common approach is to linearize the radiative response of the climate system to a given forcing perturbation about the temperature response. In the case of spatially dependent feedbacks, this linearization can be expressed locally as

$$\Delta N - \Delta F - H = \Delta R = \lambda \Delta T + O(\Delta T^2) \tag{1}$$

where H is a forcing perturbation, ΔF is the heating by anomalous atmospheric motions, ΔN is the anomalous transient energy imbalance, ΔR is the radiative response, ΔT is the temperature response, λ is a linear scaling factor, and each term is defined as a function of longitude and latitude (Hansen et al. 1985; Boer and Yu 2003a,b; Armour et al. 2012; Feldl and Roe 2013). The scaling factor λ is generally called the *local climate feedback parameter* and the temperature response ΔT is generally called the *climate sensitivity*, with their precise definitions dependent on averaging conventions. The forcing perturbation, energy imbalance, and radiative response are evaluated at an upper boundary (usually the tropopause) and the temperature response is evaluated at the surface.

The forcing-feedback framework is frequently used to explore various *thermodynamic* responses to anthropogenic forcing. It is much less commonly used to explore the *circulation* responses to anthropogenic forcing. This is important, since there is clearly a robust two-way coupling between climate feedbacks and the large-scale circulation. For example: The climate sensitivity depends on circulation-moderated patterns of surface warming (Armour et al. 2012; Andrews et al. 2014; Dong et al. 2020), and the circulation response depends on various cloud-climate feedbacks (Ceppi and Hartmann 2016; Voigt and Shaw 2015; Bony et al. 2015; Ceppi and Hartmann 2016; Li et al. 2019). A growing body of work has focused on identifying robust thermodynamic constraints on the circulation response (e.g., Shepherd 2014; Bony et al. 2015; Shaw et al. 2016; Shaw 2019), but the role of climate feedbacks on these constraints is not always clear.

The purpose of this paper is to explore the direct relationships between climate sensitivity, climate feedbacks, and the large-scale circulation. To do so, we exploit an analogy between the local climate feedback parameter and the thermal relaxation coefficient used with the "dynamical

core" of a general circulation model. The procedure allows us to quantify the importance of feedbacks – and thus climate sensitivity – for both the climatological large-scale circulation and its response to forcing perturbations. Section 2 demonstrates that the thermal relaxation coefficient used in dynamical core models is analogous to the local climate feedback parameter. This means that the climate feedbacks in dynamical core models are explicitly prescribed and exactly linear. Section 3 compares the feedbacks in a common configuration of dynamical core models with those derived from more complex models. Section 4 describes the experimental design. Sections 5 and 6 explore the influence of the climate feedbacks (and, thus, climate sensitivity) on the climatological large-scale circulation and its response to horizontally uniform forcing perturbations. Section 7 summarizes the results and discusses their implications for the circulation response to global warming.

2. Thermal relaxation and the climate feedback parameter

The *dynamical core* represents the component of any general circulation model (GCM) that evaluates the primitive equations. Held and Suarez (1994) first proposed comparing dynamical cores by replacing all entropy-increasing physics with linear relaxation terms. The resulting simplified models are called *dynamical core models*. Since their pioneering paper, dynamical core models have been used to explore a wide range of problems in extratropical variability (e.g., Boljka et al. 2018; Chen et al. 2020), as well as the extratropical circulation responses to stratospheric cooling (e.g., Kushner and Polvani 2004, 2006), tropical heating (e.g., Butler et al. 2010; Mbengue and Schneider 2013; Lu et al. 2014; Sun et al. 2013), and variations in boundary layer friction (Chen et al. 2007). Here we use a dynamical core model to probe the relationships between climate sensitivity and the extratropical circulation. We accomplish this by exploiting the close analogy between the relaxation term used in the thermodynamic equation of a dynamical core model and the canonical definition of the climate feedback parameter.

To clarify the analogy, consider the thermodynamic equation of state for a dynamical core atmosphere where all diabatic processes are parameterized as a linear relaxation of the temperature field:

$$N = F + Q = F - C\left(\frac{T - T^{e}}{\tau}\right). \tag{2}$$

Above, T is the air temperature; F is the heat transport convergence; $N \equiv C(\partial T/\partial t)$ is the transient energy imbalance; $Q \equiv -C(T-T^{\rm e})/\tau$ is the thermal relaxation rate (i.e., the diabatic heating rate), which we call the *thermal forcing*; $T^{\rm e}$ is the *equilibrium temperature*; τ is the *thermal relaxation timescale*; and $C = c_p/g$ is the heat capacity density (where c_p is the specific heat capacity at constant pressure and g is the acceleration due to gravity). The units of of N, F, and Q are $V = V^{-2} = V^{-1}$, and the units of C are $V = V^{-2} = V^{-1}$. The equilibrium temperature and thermal relaxation timescale are both defined as a function of latitude and height (i.e., they are zonally symmetric).

Now consider Equation 2 for two climate states with identical equilibrium temperature profiles: 1) a control climate in which the only forcing terms are the heat transport convergence F and the thermal relaxation rate Q; and 2) a perturbed climate additionally forced by the forcing perturbation H on the RHS of Equation 2. Taking the difference between these equations and rearranging terms yields

$$\Delta N - \Delta F - H = \Delta Q = -\frac{C}{\tau} \Delta T \tag{3}$$

where ΔN , ΔF , ΔQ , and ΔT are the differences in energy imbalance, heat transport convergence, thermal forcing, and air temperature between the two states. Comparing Equation 3 to Equation 1, it is clear that the ratio of the heat capacity to the thermal relaxation timescale is analogous to the local climate feedback parameter λ in dynamical core models. We call this term the *relaxation* feedback parameter λ_{τ} , defined

$$\lambda_{\tau} = -\frac{C}{\tau}.\tag{4}$$

Even though λ_{τ} uniquely determines the climate feedbacks in dynamical core models, we use the prefix "relaxation" to avoid confusion with climate feedbacks in more complex models. Importantly, since λ_{τ} is proportional to τ^{-1} , the climate sensitivity implied by λ_{τ} is proportional to τ (see Figure 7, B and Appendix A). An intuition for this proportionality can be gained as follows: If we group the forcing perturbation H into the numerator of the thermal relaxation term $-C(T-T^{\rm e})/\tau$ (Equation 2), it is clear that H can be equivalently expressed as the thermal relaxation timescale-scaled equilibrium temperature perturbation $\Delta T^{\rm e} \equiv H\tau/C$. Since this equilibrium temperature

perturbation is scaled by τ , and since climatological temperature is generally proportional to equilibrium temperature, it follows that τ must be generally proportional to climate sensitivity.

The central difference between the feedback parameter in complex climate models (λ in Equation 1) and the feedback parameter in dynamical core models (λ_{τ} in Equation 3) is that the former is defined with surface temperature and the radiative flux across an upper boundary, whereas the latter is defined with air temperature and the local diabatic heating. Nevertheless, the analogy between λ and λ_{τ} is important, since it means that we can explicitly prescribe the feedback parameters in a dynamical core model to assess the role of climate feedbacks on the atmospheric circulation. The approach stands in contrast to analyses of fully coupled GCM simulations, in which the feedback parameter cannot be prescribed *a priori* and must instead by diagnosed *a posteriori*.

3. Comparisons with more complex models

In our experiments with the dynamical core model, we use three globally-averaged quantities to quantify the sensitivity of each configuration to forcing perturbations (see Appendix A for details):

- 1. The reference thermal relaxation timescale $\tau_0 = 1/\overline{\langle 1/\tau \rangle}$ (Equation A6), defined as the inverse average of the inverse thermal relaxation timescale over the entire atmosphere (where the single overbar denotes a horizontal average and the single angle brackets denote a vertical average).
- 2. The *relaxation sensitivity parameter* $s_{\tau} = -1/\overline{\langle\langle \lambda_{\tau} \rangle\rangle} = \tau_0/C_0$ (Equation A6), equivalent to the negative inverse of the horizontally averaged, vertically integrated relaxation feedback parameter (where the double angle brackets denote a vertical integral and C_0 is the heat capacity of the full atmospheric column). This represents the climate sensitivity per unit forcing under the assumption of spatially uniform warming.
- 3. The *relaxation climate sensitivity* $\Delta T_{\tau} = -\overline{\langle\langle H \rangle\rangle}/\overline{\langle\langle \lambda_{\tau} \rangle\rangle} = \overline{\langle\langle H \rangle\rangle}\tau_0/C_0$ (Equation A7), equivalent to the product of the relaxation sensitivity parameter and the horizontally averaged, vertically integrated forcing perturbation. This represents the climate sensitivity under the assumption of spatially uniform warming. Empirical measures of the climate sensitivity generally scale with ΔT_{τ} under the same forcing and feedback patterns (see Section 6 and Figure 7, B).

We also use the relaxation feedback parameter λ_{τ} (Equation 1) to quantify the strength of the local climate feedbacks. Specifically, we argue that λ_{τ} can be viewed as the dynamical core-equivalent of the net radiative feedback kernel K (see Appendix A and Equation A4). Before proceeding with the experiment results, we consider how s_{τ} and λ_{τ} calculated from typical configurations of dynamical core models (see Appendix B) compare with more conventional derivations of the climate sensitivity parameter and radiative feedback kernels.

Figure 1 shows the relationship between the relaxation sensitivity parameter s_{τ} and the reference thermal relaxation timescale τ_0 (solid black line). Under the common Held and Suarez (1994; hereafter HS94) configuration used with dynamical core models (Appendix B), the relaxation sensitivity parameter s_{τ} is approximately $0.2\,\mathrm{K/W\,m^{-2}}$ (Figure 1, dashed black line). This is lower than consensus estimates from versions 5 and 6 of the Coupled Model Intercomparison Project (CMIP), as the HS94 configuration was not designed with the goal of producing a realistic climate sensitivity. To match the CMIP estimates, the reference relaxation timescale would need to be on the order of 100 days rather than 20 days (Figure 1, blue and red lines and shading; Zelinka et al. 2020). Notably, the HS94 relaxation sensitivity parameter is also lower than two separate estimates of the Planck sensitivity parameter: The first obtained from CMIP simulations of global warming (Zelinka et al. 2020), the second from applying the Stefan-Boltzmann Law to climatological temperatures under the HS94 configuration (see Equation A8). Both Planck estimates imply a reference thermal relaxation timescale on the order of 40 days rather than 20 days (Figure 1, gray lines). Figure 1 motivates us to study the effects of longer relaxation timescales on the large-scale circulation (Section 5).

Figure 2 compares the latitude-height profile of the HS94 relaxation feedback parameter λ_{τ} (Figure 2, D) against clear-sky temperature, specific humidity, and combined temperature-specific humidity radiative feedback kernels (Figure 2, A–C; see Equation A5) estimated by Huang et al. (2017) from the ERA-Interim reanalysis data set (Dee et al. 2011). The specific humidity radiative kernel is scaled by the specific humidity change associated with a 1 K temperature perturbation under constant relative humidity, consistent with the Clausius-Clapeyron relation (e.g., Held and Soden 2006). The average magnitude of the relaxation feedback parameter given by the HS94 configuration is about 20% that of the combined temperature-specific humidity ERA-Interim radiative kernel (Figure 2, C–D; note the separate color scales). This is more-or-less consistent

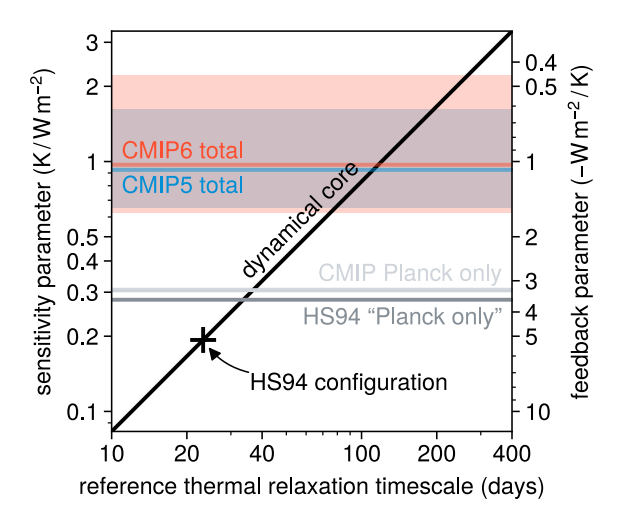


Fig. 1. Climate sensitivity and the thermal relaxation timescale. (black, solid) The relaxation sensitivity parameter s_{τ} as a function of the reference thermal relaxation timescale τ_0 in a dynamical core model, with the Held and Suarez (1994; hereafter HS94) configuration indicated by the plus marker. (dark gray) The Planck climate sensitivity parameter from the HS94 configuration, using the atmosphere-average temperature as the "emission" temperature (see Appendix A and Equation A8). (light gray) The Planck climate sensitivity parameter diagnosed from the consensus of CMIP abrupt 4×CO₂ experiments ($s_0 \approx 0.3 \,\text{K/W}\,\text{m}^{-2}$, $\Delta T_0 \approx 1.2 \,\text{K}$; e.g., Zelinka et al. 2020). (blue and red) The mean (solid lines) and 5-95 percentile range (shading) net climate sensitivity parameter diagnosed from the CMIP5 (blue) and CMIP6 (red) abrupt 4×CO₂ experiments (Zelinka et al. 2020; data obtained online via Zelinka 2021). The right y-axis shows the feedback parameter λ associated with each sensitivity parameter s (i.e., the negative inverse sensitivity parameter).

with Figure 1 (compare dashed black lines with blue and red lines, right y-axis). But notably, the spatial pattern of the HS94 relaxation feedback parameter compares favorably with that of the temperature-specific humidity radiative kernel in the lower and middle troposphere (Figure 2, C–D). Both are characterized by a weakly negative feedback throughout the middle troposphere and much stronger negative feedbacks in the lower troposphere at low latitudes. The ERA-Interim radiative feedback kernel is locally amplified due to the combined effects of a strong vertical gradient in the scaled specific humidity radiative kernel and a strong meridional gradient in the temperature radiative kernel (Figure 2, A–B). By contrast, the HS94 relaxation feedback parameter was locally amplified by Held and Suarez (1994) in order to roughly match real-world circulation statistics and thermal stratification. It is not entirely clear whether the goal of producing a realistic steady-state

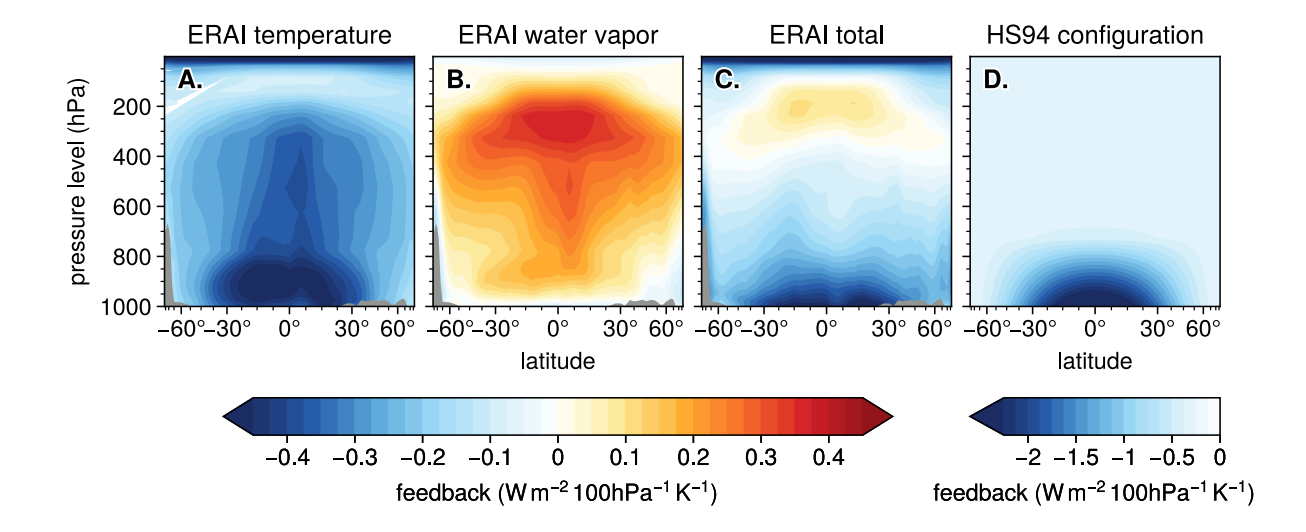


Fig. 2. Radiative feedback kernels and the thermal relaxation timescale. (A) The annual-mean zonal-mean air temperature radiative feedback kernel K_T from the ERA-Interim reanalysis data set (ERAI; Dee et al. 2011), estimated as the top-of-atmosphere radiative response to a 1 K temperature perturbation as a function of the latitude and height of the applied perturbation (Huang et al. 2017; data obtained online via Huang 2022). The radiative response is normalized by the average pressure thickness of the perturbed model level, and only the clear-sky component of the response is shown (i.e., cloud radiative effects were excluded from the radiative transfer calculations; Huang et al. 2017). Pressures above the 0.33 quantile surface pressure are masked out with gray, and the x-axis is scaled by a sine function so that equal distances along the axis correspond to equal spherical surface areas. (B) As in A, but for the radiative response to the specific humidity perturbations required for a constant-relative humidity response to a 1 K temperature perturbation. This represents the specific humidity radiative feedback kernel K_q multiplied by the Clausius-Clapeyron scaling $\partial q/\partial T$ (Equation A5); thus, the units also have Kelvin in the denominator. (C) As in A, but for the combined temperature-specific humidity radiative feedback kernel $K_{T,q}$ (equivalent to the sum of panels A and B; Equation A5). (D) The relaxation feedback parameter $\lambda_{\tau} = -c_p/g\tau$ from the Held and Suarez (1994) configuration (please note the distinct color scale).

climate necessarily guarantees a realistic pattern of relaxation feedback parameters, or whether the resemblance of the HS94 relaxation feedback parameters to the clear-sky radiative feedback kernel is a coincidence. Regardless, as shown later, the non-uniformity of the relaxation feedback parameter turns out to play a critical role in governing the circulation response to horizontally uniform forcing perturbations (Section 6).

4. Experimental design

To study the effects of relaxation climate sensitivity on the large-scale circulation, we performed two experiments. The first experiment tests the influence of relaxation climate sensitivity on the unperturbed steady-state circulation (the unperturbed experiment), while the second experiment tests the influence of relaxation climate sensitivity on the response of the circulation to a horizontally uniform forcing perturbation (the perturbed experiment).

The *unperturbed* experiment consists of control-like simulations with relaxation climate sensitivity (i.e., thermal relaxation timescales) varying across three orders of magnitude. We first ran the model with the latitude-height fields of the equilibrium temperature and thermal relaxation timescale configured according to HS94 (Figure 3, A–B; see Appendix B). In the HS94 configuration, the equilibrium temperature T^e is characterized by large meridional temperature gradients, a statically neutral lapse rate at the poles, and a statically stable lapse rate at the equator (Figure 3, A; Equation B1); the thermal relaxation timescale τ is characterized by a minimum of τ_{min} = 4 days at the surface on the equator and a maximum of τ_{max} = 40 days above ~700hPa and at the poles (Figure 3, B; Equation B2). We then perturbed the relaxation climate sensitivity by uniformly scaling the thermal relaxation timescale τ ; the maximum relaxation timescale τ_{max} used with each simulation was 0.4, 1, 2, 4, 10, 20, 30, 40, 50, 60, 80, 100, 120, 160, 200, and 400 days, and the minimum relaxation timescale τ_{min} was always one tenth the maximum relaxation timescale τ_{max} (consistent with HS94; Equation B2).

The *perturbed* experiment consists of simulations with forcing perturbations imposed upon a subset of the unperturbed simulations. Since we cannot increase the optical depth or greenhouse gas concentration in a dynamical core model, we instead perturbed the model with a horizontally uniform, vertically decaying forcing perturbation H (Figure 3, C) analogous to a greenhouse gas radiative forcing perturbation:

$$H = h_0 C \left(\frac{p}{p_0}\right)^{\kappa} \tag{5}$$

Above, p is the pressure, $p_0 \equiv 10^5 \, \text{Pa}$ is the reference pressure, h_0 is the reference heating in units K/day, $C = c_p/g$ is the heat capacity density (see Equations 2 and 3), and $\kappa \equiv R_{\rm d}/c_p$ is the Poisson constant (where $R_{\rm d}$ is the dry air gas constant). The vertical structure of the perturbation

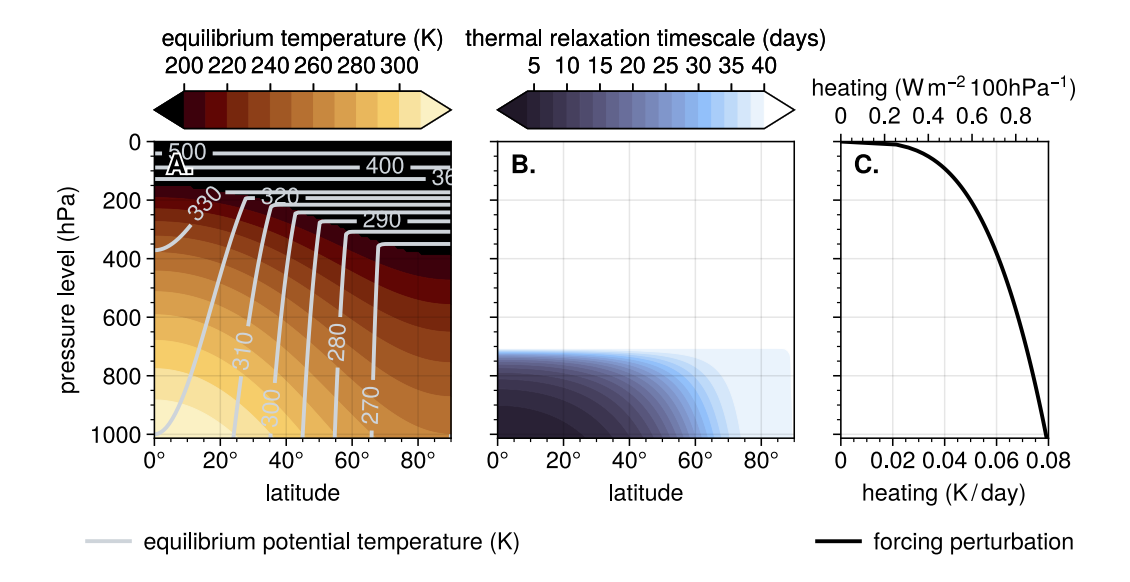


Fig. 3. **Dynamical core model forcing terms.** Latitude-height cross-sections of the (A) equilibrium temperature T^e and (B) thermal relaxation timescale τ used to drive thermal forcing under the Held and Suarez (1994) configuration of a dynamical core model (Equations B1 and B2). The light gray contours in panel A indicate the potential temperatures $\theta^e \equiv T^e(p_0/p)^\kappa$ associated with the equilibrium temperature field. (C) Vertical profile of the "global warming" thermal forcing perturbation H (Equation 5).

is designed to mimic the effect of perturbing the global average surface equilibrium temperature \overline{T}_s^e (compare Equation 5 with Equation B1). The reference heating h_0 was set to 0.079 K/day, such that the vertically integrated forcing perturbation is equivalent to the CMIP5 consensus for the radiative forcing perturbation due to an instantaneous quadrupling of CO₂ (Andrews et al. 2012): $\langle\!\langle H \rangle\!\rangle = h_0 p_0 C (p_s/p_0)^{\kappa+1} (\kappa+1)^{-1} = 7.4 \text{ W m}^{-2}$, where $p_s = 101325 \text{ Pa}$ is the global average surface pressure and the double angle brackets denote a vertical integral.

We used the forcing perturbation H rather than a perturbation in the global average surface equilibrium temperature \overline{T}_s^e (Equation B1) because the magnitude of the response to any equilibrium temperature perturbation ΔT^e is independent of relaxation climate sensitivity. It can be seen from Equations 2 and 3 that any perturbation ΔT^e is equivalent to the constant heating term $\hat{H} = -\lambda_\tau \Delta T^e$. Since the magnitude of this heating is scaled by the strength of the feedback $\lambda_\tau = -C/\tau$, the temperature response is always independent from the relaxation climate sensitivity. The heating term H is thus more appropriate than \hat{H} for investigating links between relaxation climate sensitivity and the large-scale circulation.

5. Relaxation climate sensitivity and the unperturbed circulation

Figure 4 summarizes the climatological large-scale circulation under different relaxation climate sensitivities. In general, lower relaxation climate sensitivities (i.e., shorter thermal relaxation timescales) are associated with stronger thermal forcing (i.e., larger thermal relaxation rates; Figure 4, D-F, shading), increased baroclinicity (Figure 4, A-C, shading), intensified eddy static energy transport (Figure 4, D-F, contours), and a faster jet stream (Figure 4, A-C, black contours). That is, reducing the relaxation climate sensitivity of a dynamical core model tends to invigorate the large-scale circulation. This relationship arises from the dual role of relaxation climate sensitivity in governing both the strength of the forcing toward the baroclinically unstable equilibrium state (Figure 3, A; Equation B1) and the amplitude of the temperature anomalies resulting from external forcing perturbations.

For example, consider the climatological thermal forcing \widetilde{Q} in a dynamical core model (Equation 2):

$$\widetilde{Q} = -C\left(\frac{\widetilde{T} - T^{e}}{\tau}\right) \tag{6}$$

where the tilde indicates a climatological time average. The direct effect of reducing the relaxation climate sensitivity (and, thus, the thermal relaxation timescale τ) is to amplify the thermal forcing \widetilde{Q} (Figure 4, D–F, shading; Figure 5, A, dashed line). But there is also an indirect effect, by which reducing τ increases the meridional temperature gradient and decreases the climatological temperature \widetilde{T} at high latitudes (Figure 4, A–C, shading), as the static energy transport becomes less effective at wiping out deviations from the equilibrium state T^e . Thus, the indirect effect of reducing τ is to suppress the thermal forcing \widetilde{Q} by reducing $\widetilde{T}-T^e$ in the extratropics (Figure 5, A, dotted line). Taken together, the direct effect of reducing τ dominates the indirect effect for $\tau \gtrsim 2$ days, as the energy transport by eddies is able to sustain significant deviations from T^e (Figure 4, D–F, contours; Figure 5, A, solid line). The indirect effect is only dominant for $\tau \lesssim 1$ day, where the energy transport is unable to sustain significant deviations from the baroclinically unstable state T^e (Figure 5, A, solid line). At such short timescales, the relaxation rates exceed the maximum growth rates of baroclinic disturbances, and the energy transport shuts off.

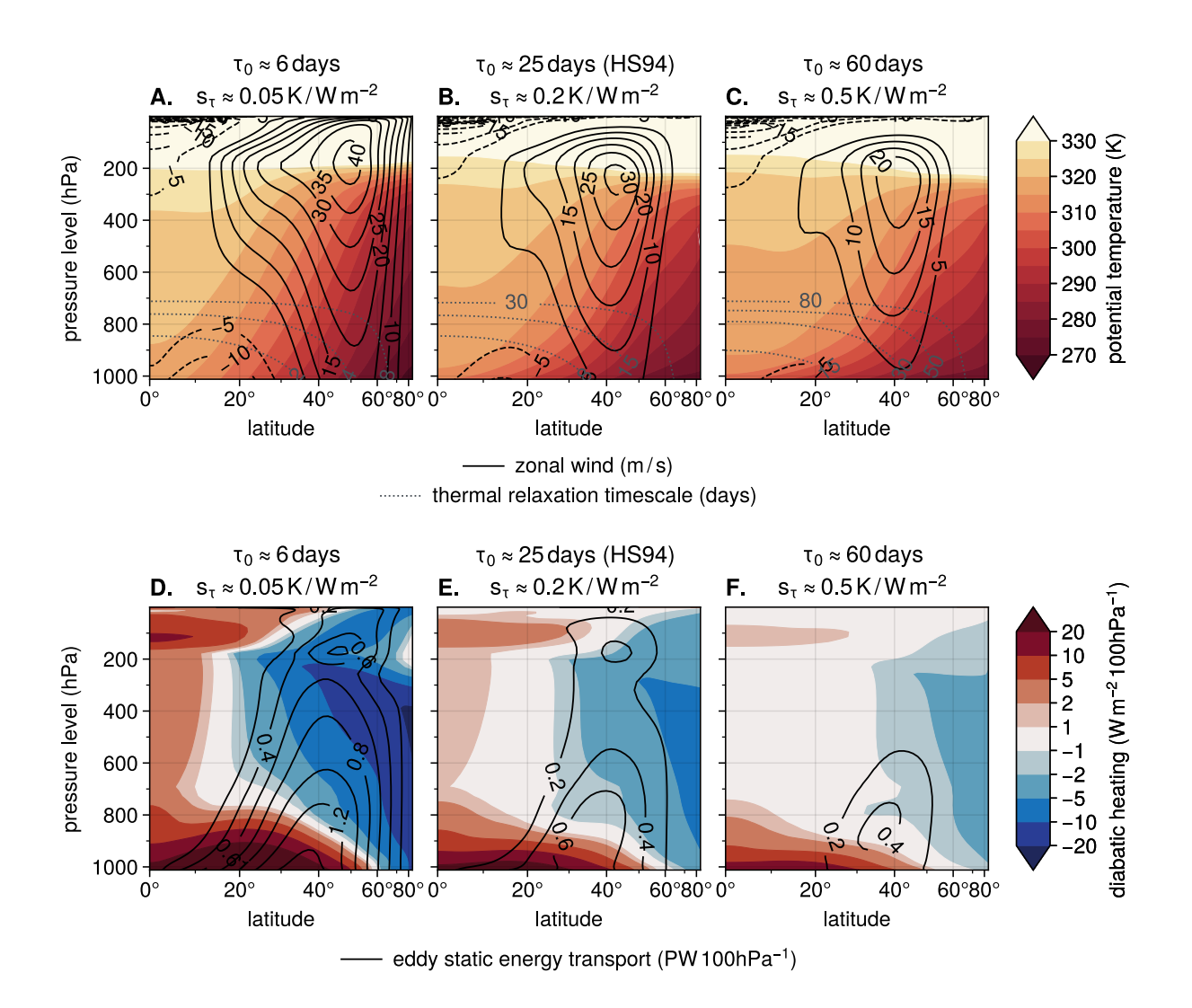


Fig. 4. Relaxation climate sensitivity and the large-scale circulation. Average latitude-height cross-sections from simulations with relaxation climate sensitivities (A, D) less than, (B, E) equal to, and (C, F) greater than the Held and Suarez (1994) relaxation climate sensitivity. The top row (A–C) shows the zonal-mean potential temperature (shading) and zonal wind (contours). The thermal relaxation timescales are shown with gray dotted contours. The bottom row (D–F) shows the zonal-mean diabatic heating rate (i.e., thermal relaxation rate; shading) and eddy static energy transport (contours). The relaxation sensitivity parameters and associated reference thermal relaxation timescales are indicated above each panel.

At steady state, the static energy transport responsible for sustaining $\widetilde{T} - T^e$ must balance the associated thermal forcing \widetilde{Q} . At high latitudes, the energy transport required to balance \widetilde{Q} is dominated by the eddies rather than the zonal-mean transport (compare solid medium gray and

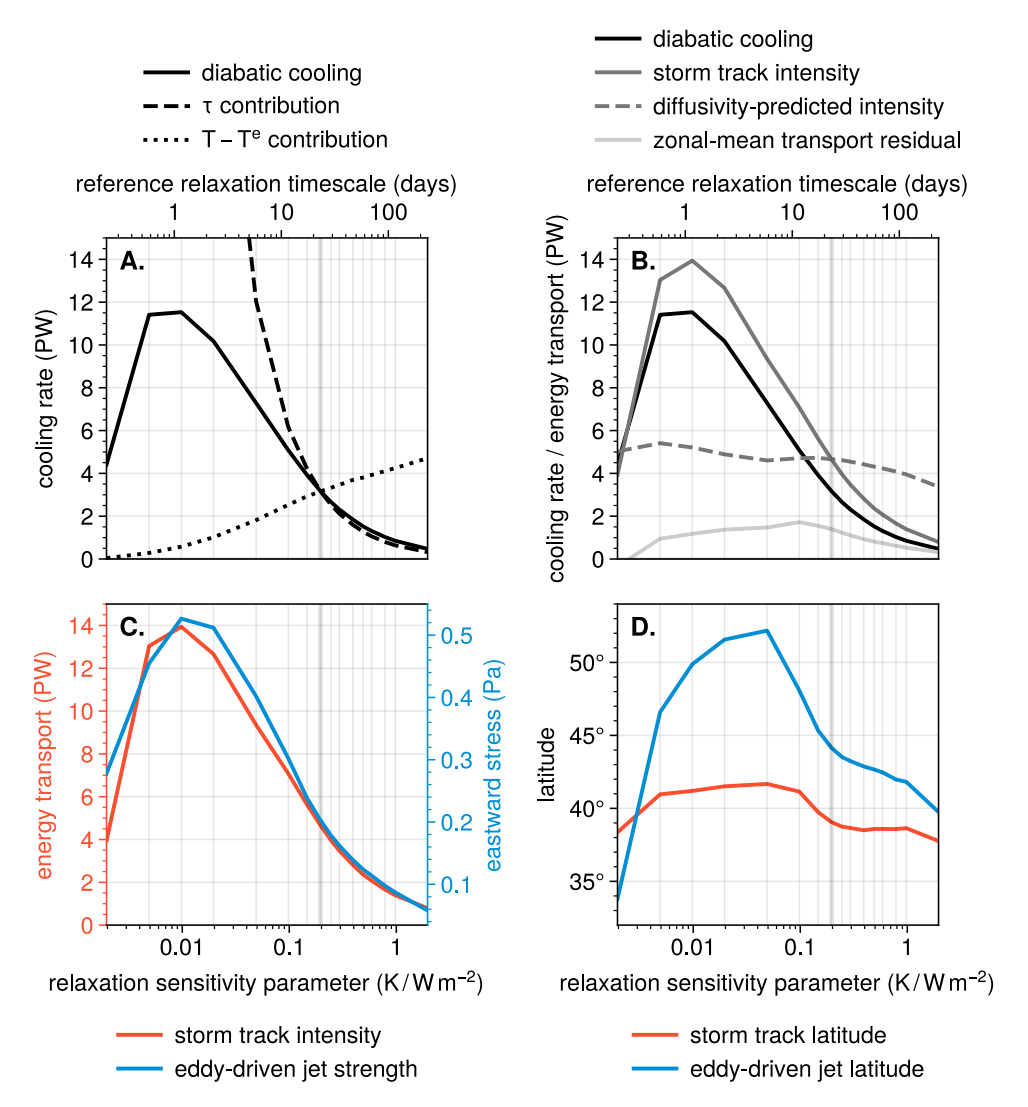


Fig. 5. **Relaxation climate sensitivity and the extratropical circulation.** Average extratropical circulation metrics as a function of the relaxation sensitivity parameter s_{τ} (bottom x-axis) and the reference thermal relaxation timescale τ_0 (top x-axis). (A) The vertically integrated diabatic cooling (i.e., negative thermal relaxation rate) integrated from the storm track to the pole, where the storm track is defined as the maximum vertically integrated eddy static energy transport. The dashed and dotted lines indicate the individual contributions of the denominator and numerator of Equation 2 to changes in net cooling relative to the Held and Suarez (1994; hereafter HS94) configuration, calculated as the diabatic cooling resulting from setting the climatological temperatures (dashed line) and relaxation timescales (dotted line) to their HS94 values. (B) The diabatic cooling from panel A (black), the storm track intensity (medium gray), and the residual due to energy transport by the zonal-mean circulation (calculated as the storm track intensity minus the diabatic cooling; light gray). The dashed gray line indicates the storm track intensity predicted by the HS94 static energy diffusivity (calculated as the product of the 850 hPa meridional static energy gradient at the storm track with the ratio of storm track intensity to static energy gradient from HS94). (C) The storm track (red) and eddy-driven jet (blue) latitudes. The configurations we explicitly tested are indicated with vertical grid lines, and the HS94 configuration is indicated with the thick vertical grid line. The eddy-driven jet is defined in Section 5.

light gray lines, Figure 5, B). Notably, the response of the eddy component of the transport to changing relaxation timescales does not follow a simple, constant-diffusivity closure. Instead, reduced relaxation climate sensitivity is associated with increased static energy diffusivity (defined as the ratio of the 850 hPa meridional static energy gradient to the vertically integrated eddy static energy transport; compare solid and dashed medium gray lines, Figure 5, B). Since shorter thermal relaxation timescales (i.e., lower relaxation climate sensitivities) tend to amplify the thermal forcing, and since amplified forcing must be balanced by increased energy transport, it is clear in general that lower relaxation climate sensitivity must be associated with a more vigorous large-scale circulation.

The influence of relaxation climate sensitivity on the large-scale circulation is manifest in two key features of the extratropical circulation: the storm track and the eddy-driven jet. Following Shaw et al. (2018), we define the "storm track" as the maximum vertically integrated eddy static energy transport $F_E = 2\pi a \cos \phi \langle [v^*s^*] \rangle$ (where a is the Earth radius; ϕ is the latitude; v is the meridional wind; $s = c_p T + \Phi$ is the static energy, where c_p is the specific heat at constant pressure and Φ is the geopotential; and the square brackets and asterisks denote the zonal average and deviations thereof, respectively). This metric captures the same internal variations as more common storm track metrics (see Shaw et al. 2018, Appendix A), but also lets us connect storm track changes to the static energy budget, since the latitudinal maximum in $F_{\rm E}$ must be balanced by the zonal-mean static energy transport $F_{\rm M} = 2\pi a \cos \phi \langle [v] \rangle \langle [s] \rangle$ at the storm track and the thermal forcing Q integrated from the storm track to the pole (Shaw et al. 2018; Figure 5, solid lines). Note that stationary eddy transport is zero in the HS94 configuration of a dynamical core model since the topography and forcing parameters are zonally uniform. Similarly, we define the "eddy-driven jet" as the maximum vertically integrated eddy angular momentum flux forcing of the zonal-mean zonal wind budget $M_E = \partial_\phi \left(\cos^2\phi \left\langle \left[v^*u^*\right]\right\rangle \right) / a\cos^2\phi$. This metric captures the same internal variations as the "surface wind maximum" definition, but is insensitive to changes in vertical shear within the friction layer (i.e., below ~700 hPa; Held and Suarez 1994).

A key result is that the intensities and latitudes of the storm tracks and eddy-driven jets are both dependent on relaxation climate sensitivity (Figure 5, C–D). Notably, this dependence is non-monotonic: The storm track and eddy-driven jet intensities are maximized for relaxation climate sensitivities around $s_{\tau} \approx 0.01 \, \text{K/W} \, \text{m}^{-2}$ (i.e., $\tau_0 \approx 1$ day; Figure 5, C). At these values,

the tendency of strong thermal forcing to invigorate the circulation is countered by its tendency to suppress baroclinic eddy growth. Interestingly, the latitudes of the storm track and eddy-driven jet are maximized for larger relaxation climate sensitivities around $s_{\tau} \approx 0.05 \, \text{K/W m}^{-2}$ (i.e., $\tau_0 \approx 5$ days; Figure 5, D). While the storm track and eddy-driven jet intensities scale mostly in tandem across the range of sampled relaxation climate sensitivities (Figure 5, C), the eddy-driven jet latitude is much more dependent on relaxation climate sensitivity than the storm track latitude (Figure 5, D).

The pronounced influence of relaxation climate sensitivity on the extratropical circulation suggests that the circulation characteristics of more complex models might also be linked to their climate sensitivity. Such relationships could be used to construct *emergent constraints* on multimodel estimates of climate sensitivity (e.g., Klein and Hall 2015; Hall et al. 2019). We can test the likelihood that a circulation characteristic might serve as a useful emergent constraint by comparing its dependence on relaxation climate sensitivity with its dependence on equilibrium temperature. Since equilibrium temperature is independent from relaxation climate sensitivity (Equation 2), a circulation characteristic that is strongly dependent on equilibrium temperature is less likely to be a unique indicator of climate sensitivity. A more realistic analogue for this might be circulation differences arising from model disagreements in radiative-convective equilibrium temperature that are independent of climate sensitivity.

To test the dependence of the circulation on equilibrium temperature, we carried out an additional experiment holding the thermal relaxation timescale fixed and running the model with surface equator-pole equilibrium temperature differences Δ_h^e of 10, 20, 40, 60, 90, 120, and 150 K (Equation B1). Figure 6 compares extratropical circulation characteristics from the relaxation climate sensitivity experiment (blue lines) and equilibrium temperature experiment (orange lines) as a function of the diabatic cooling integrated from the storm track to the pole (i.e., the black line in Figure 5, B). Perturbations in equilibrium temperature clearly lead to significant responses in both the storm track and eddy-driven jet intensity (Figure 6, orange lines). Importantly, a nearly identical circulation response results from perturbations in either the equilibrium temperature or relaxation climate sensitivity, as long as their effects on the thermal forcing constraint are identical (compare orange and blue lines, Figure 6). This suggests that while relaxation climate sensitivity

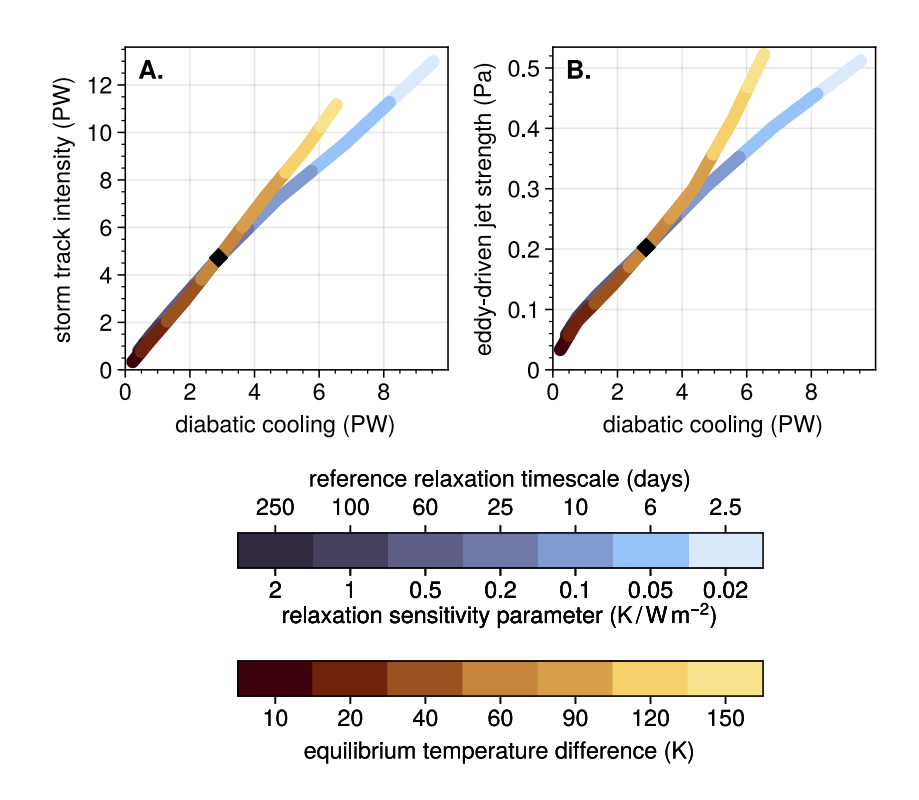


Fig. 6. **Thermodynamic constraints on the extratropical circulation.** Each distinct line segment represents the steady-state climatology from a simulation where the relaxation climate sensitivity (i.e., reference thermal relaxation timescale; blue) or surface equator-pole equilibrium temperature difference (orange) was perturbed relative to the Held and Suarez (1994) configuration (indicated by the black diamond). The lines can be thought of as parametric functions of the *x*- and *y*-axis variables, where the independent variable (the forcing parameter) is indicated by the position along the line. For each panel, the *x*-axis indicate vertically integrated diabatic cooling, integrated from the storm track to the pole (see Figure 5, B). The *y*-axes indicate the (A) storm track intensity and (B) eddy-driven jet strength (as defined in Section 5). Where the *y*-axis parameter is constrained by the diabatic cooling, the orange and blue lines should coincide. Where the *y*-axis parameter is constrained by the relaxation climate sensitivity, the orange line should be horizontal.

plays an important role in determining the extratropical circulation, it is unlikely that circulation intensity could be used to construct a useful emergent constraint on climate sensitivity.

In sum, Figures 4–6 demonstrate that relaxation climate sensitivity plays a central role in governing the structure and amplitude of the large-scale circulation. Lower relaxation climate sensitivities (i.e., shorter relaxation timescales) lead to a more vigorous extratropical circulation by strengthening the thermal forcing. The relationship only breaks down for extremely low relaxation climate

sensitivities, under which baroclinic eddies are unable to grow. In the following section, we explore the implications of these results for the large-scale circulation response to global warming.

6. Relaxation climate sensitivity and the perturbed circulation

In addition to the unperturbed simulations, we carried out several perturbed "global warming" simulations using a wide range of relaxation climate sensitivities. This was done by imposing a horizontally uniform heating term analogous to a greenhouse gas radiative forcing perturbation (see Section 4 for details). The perturbed simulations provide insight into the role of relaxation climate sensitivity in governing the large-scale circulation response to global warming.

By construction, given the same forcing perturbation H, the dynamical core responds with greater warming for model configurations with higher relaxation climate sensitivity (Figure 7, B; Figure 8, A–C, shading). The simulated warming scales almost linearly with respect to the reference sensitivity parameter, whether averaged over the entire atmosphere or a near-surface layer (Figure 7, B, red dashed and dotted lines). However, the magnitude of the warming deviates slightly from that predicted by the reference sensitivity parameter (Figure 7, B, black solid line). This is due to the non-zero spatial covariance between the temperature response and the relaxation feedback parameter (compare shading and dotted contours, Figure 8, A–C), which decreases the full-atmosphere effective feedback parameter $\hat{\lambda}_{i\tau}$ (Equation A1) and increases the near-surface effective feedback parameter $\hat{\lambda}_{i\tau}$ (Equation A2). The results described here represent *steady-state* responses, since the diabatic cooling anomalies integrated over the entire atmosphere are equivalent to the imposed forcing perturbation $\overline{\langle H \rangle}$ (Figure 7, A, red and black lines).

The dynamical core model captures the basic qualitative structure of the warming response from more complex general circulation models: There is enhanced warming near the polar surface, analogous to polar amplification (Figure 8, A–C, shading; e.g., Holland and Bitz 2003; Alexeev et al. 2005; Crook et al. 2011; Pithan and Mauritsen 2014), and enhanced warming in the tropical upper troposphere, analogous to moist adiabatic adjustment (Figure 8, A–C, shading; e.g., Held and Soden 2000, 2006; O'Gorman and Muller 2010). The warming pattern is similar for all simulations, but larger in magnitude for simulations with higher relaxation climate sensitivity. Importantly, when we repeat the unperturbed and perturbed experiments with spatially uniform relaxation feedback parameters (accomplished by setting $\tau_{min} = \tau_{max}$; Equations 4 and B2), the warming is virtually

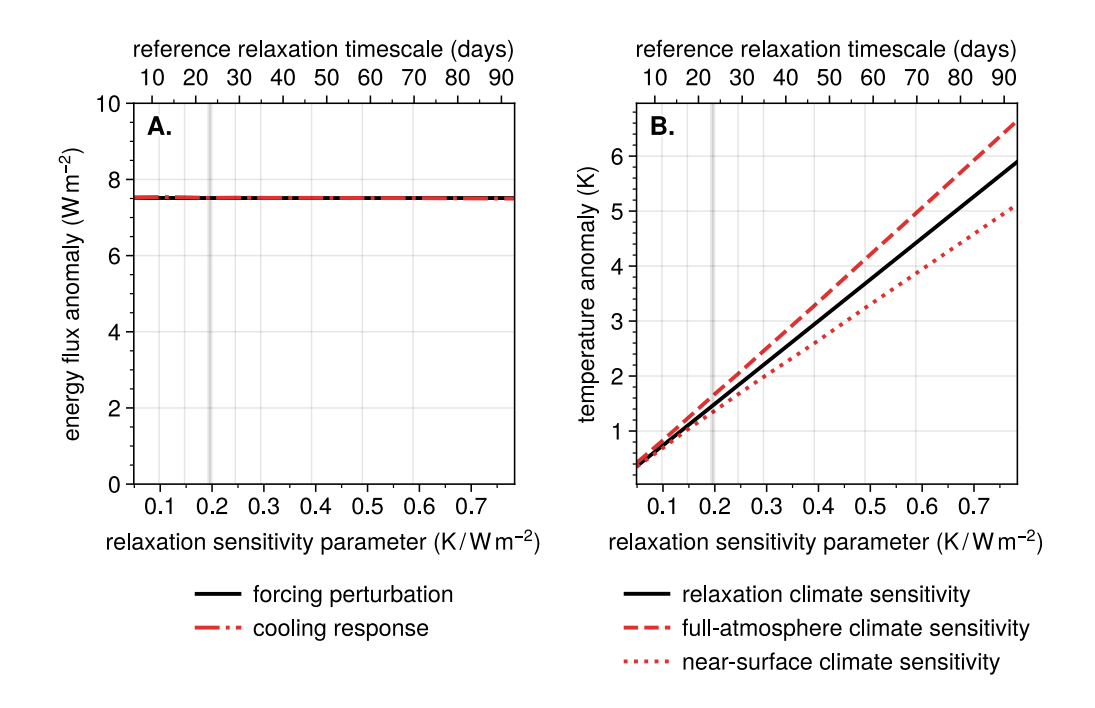


Fig. 7. Relaxation climate sensitivity and the thermodynamic response to global warming. (A) The global average vertical integral of the imposed forcing perturbation H (solid black; Equation 5) and the simulated diabatic cooling response ΔQ (i.e., negative thermal relaxation response; dash-dotted red; Equation 3). (B) The prescribed relaxation climate sensitivity ΔT_{τ} (solid black; Equation A7) and the simulated temperature response ΔT averaged over the entire atmosphere (dashed red; Equation A1) and over the near-surface 900 hPa pressure level (dotted red; Equation A2). Note that the black lines indicate quantities prescribed *a priori* and the red lines indicate quantities diagnosed from simulations. The configurations we explicitly tested are indicated with vertical grid lines, and the Held and Suarez (1994) configuration is indicated with the thick vertical grid line.

horizontally uniform and decays with height according to H (compare Figures 8 and 9, A–C and Figure 3, C).

The agreement with more complex models in the qualitative warming pattern may appear surprising given that the dominant physics creating this pattern (i.e., increased latent heat release, moisture transport changes, and ice-albedo feedback) are not represented in the dynamical core model. They come about somewhat fortuitously due to the non-uniform pattern of relaxation feedback parameters (i.e., thermal relaxation timescales; Figure 8, A–C, dotted contours). In particular, the enhanced polar lower-tropospheric warming appears to derive from meridional gradients in the relaxation feedback parameter (compare shading and dotted contours, Figure 8, A–C), analogous

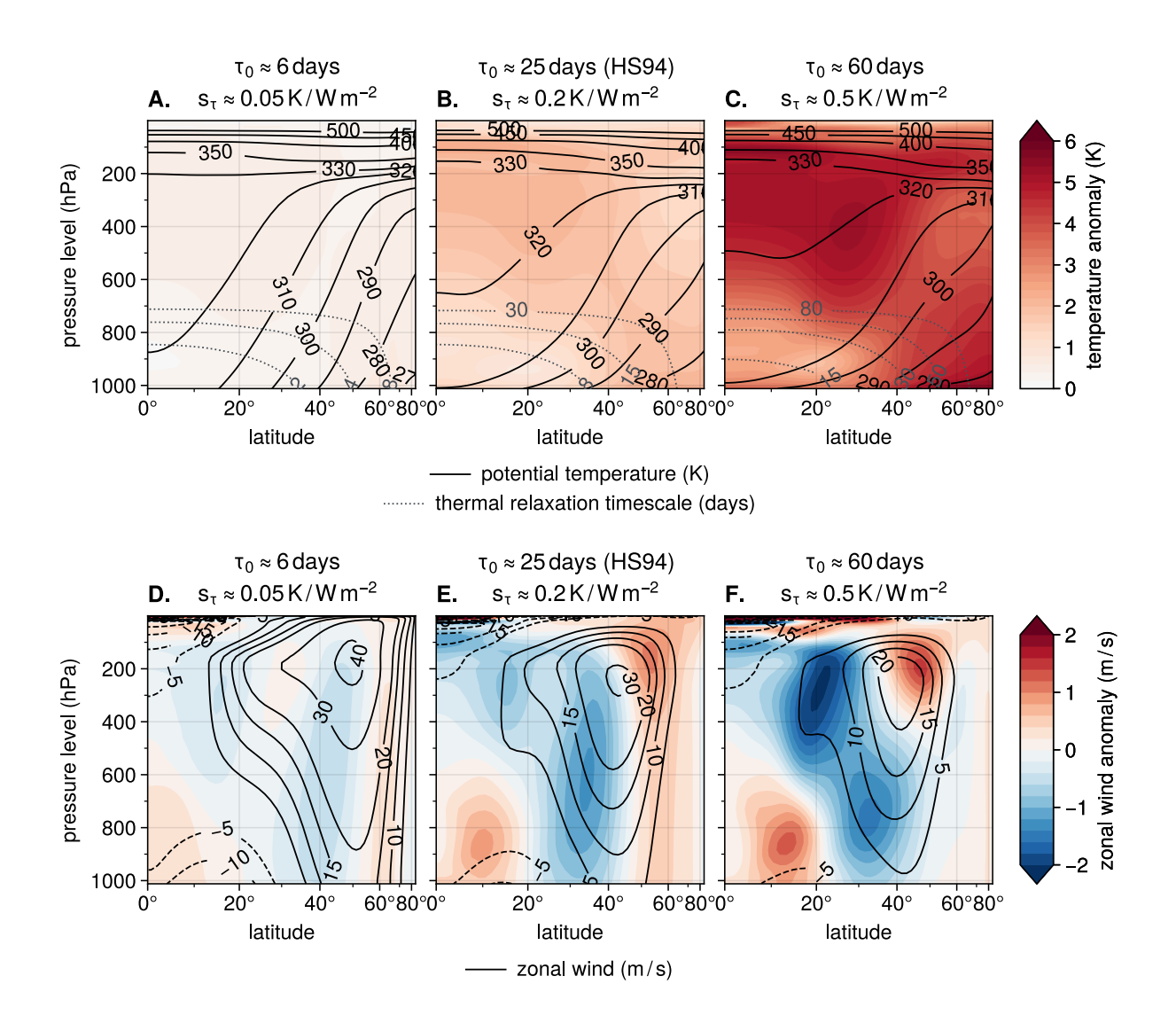


Fig. 8. Relaxation climate sensitivity and the large-scale circulation response to global warming. Steady-state latitude-height cross-sections from the global warming simulations with relaxation climate sensitivities (A, D) less than, (B, E) equal to, and (C, F) greater than the Held and Suarez (1994) relaxation climate sensitivity. The top row (A–C) shows the unperturbed zonal-mean potential temperature (contours) and the temperature response to the forcing perturbation (shading). The thermal relaxation timescales are shown with gray dotted contours. The bottom row (D–F) shows the unperturbed zonal-mean zonal wind (contours) and the zonal wind response to the forcing perturbation (shading). The relaxation sensitivity parameters and associated reference thermal relaxation timescales are indicated above each panel.

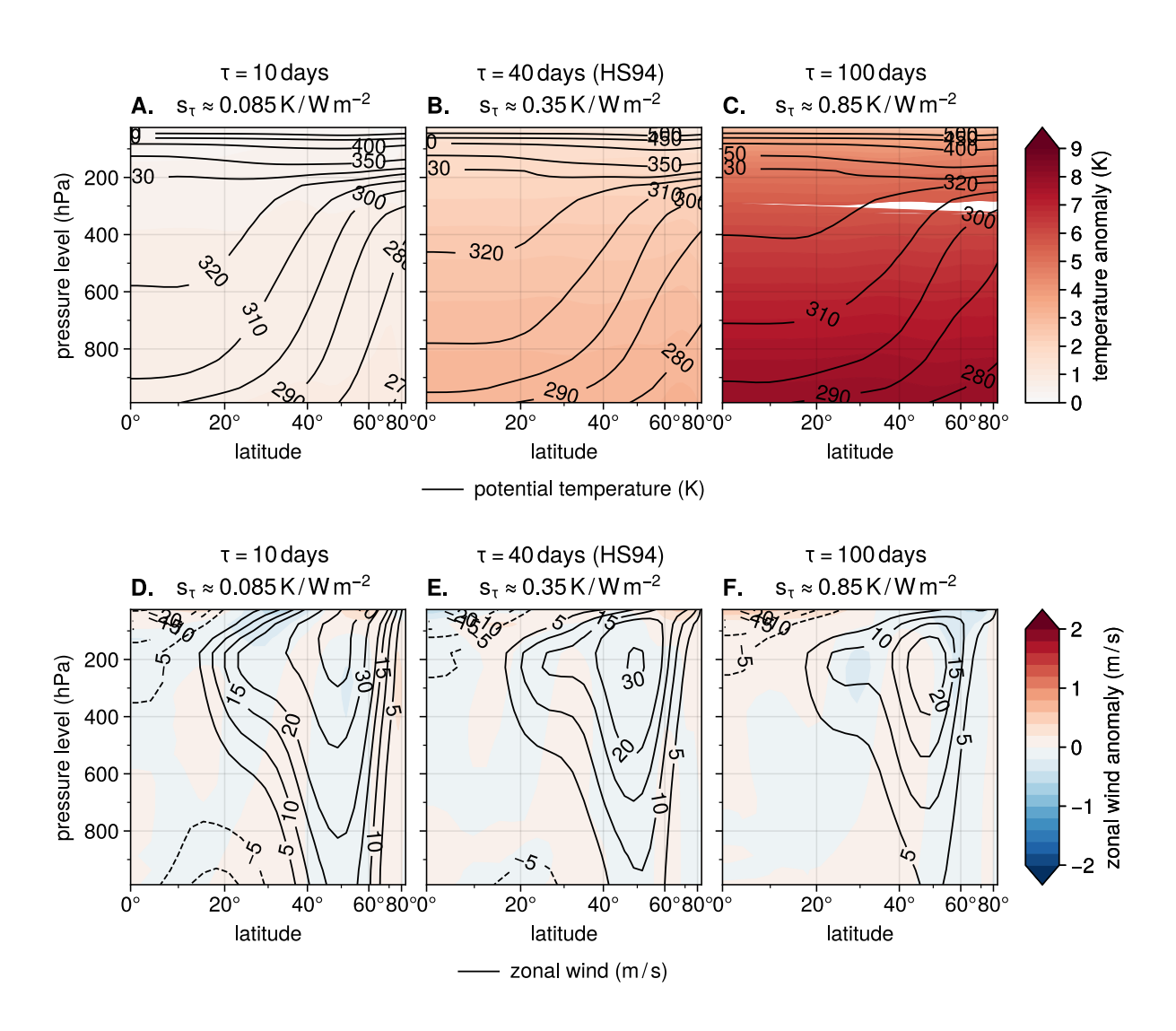


Fig. 9. As in Figure 8, but for the experiments with uniform thermal relaxation timescales.

to meridional gradients in the temperature radiative kernel (Figure 2, A and D). Similarly, the enhanced tropical upper-tropospheric warming appears to derive from vertical gradients in the relaxation feedback parameter, (compare shading and dotted contours, Figure 8, A–C), analogous to vertical gradients in the Clausius-Clapeyron-scaled specific humidity radiative kernel (Figure 2, B and D).

The warming response to the forcing perturbation H is associated with notable changes in the large-scale circulation. The storm track and the eddy-driven jet both shift poleward, with a generally larger shift for model configurations with higher relaxation climate sensitivity (Figure 10, C–D). For every climate sensitivity, the spatial pattern of the zonal wind response is characterized by a

deceleration of the equatorward flank of the eddy-driven jet and a deceleration of the upper-level subtropical jet extension (Figure 8, D–F, shading). The responses scale with relaxation climate sensitivity because under a fixed pattern of relaxation feedback parameters, higher relaxation climate sensitivity corresponds to larger horizontal temperature gradient anomalies (Figure 8, A–C, shading). In the case of spatially uniform relaxation feedback parameters, where there are no changes to the horizontal temperature gradient (Figure 9, A–C, shading), the zonal wind response and poleward storm track and eddy-driven jet shifts entirely disappear (compare Figures 8 and 9, D–F; Figures 10 and 11, C–D).

The warming response is also associated with a robust reduction in storm track intensity (Figure 10, A–B, red lines). At first glance, the increased temperature gradients in the middle and upper troposphere would seem to imply an increase in storm track intensity (Figure 8, A–C, shading). However, since the thermal relaxation coefficients are stronger in the boundary layer, changes to the temperature gradients in the lower troposphere result in comparatively larger changes to the thermal forcing. Thus, the lower tropospheric temperature gradients play an outsize role in determining the total heat transport response. The magnitude of the response is small due to the competing effects of the decreased lower troposphere temperature gradients and increased middle and upper troposphere temperature gradients, again analogous to more complex models (Shaw et al. 2016). In the case of spatially uniform relaxation feedback parameters, since there is no meridional contrast in the thermal forcing response, the storm track intensity reduction disappears (compare Figures 10 and 11, A–B, red lines).

Notably, whereas the zonal wind response and latitude shifts depend on relaxation climate sensitivity, the storm track intensity response does not (Figure 10, B, red line). This is due to the fact that 1) the latitude-height thermal relaxation coefficient pattern (i.e., relaxation feedback parameter pattern; Figure 2, D) is unchanged between model configurations (Figure 8, A–C, dotted contours) and 2) the global average thermal forcing response is necessarily constant (Figure 7, A, red line). While the global warming forcing perturbation always increases global temperature and decreases near-surface meridional temperature gradients, the magnitude of the temperature change is scaled everywhere by the relaxation feedback parameter. Thus, the thermal forcing response associated with the temperature change is roughly constant. Since the storm track intensity is constrained by thermal forcing, the storm track response to the forcing perturbation is necessarily

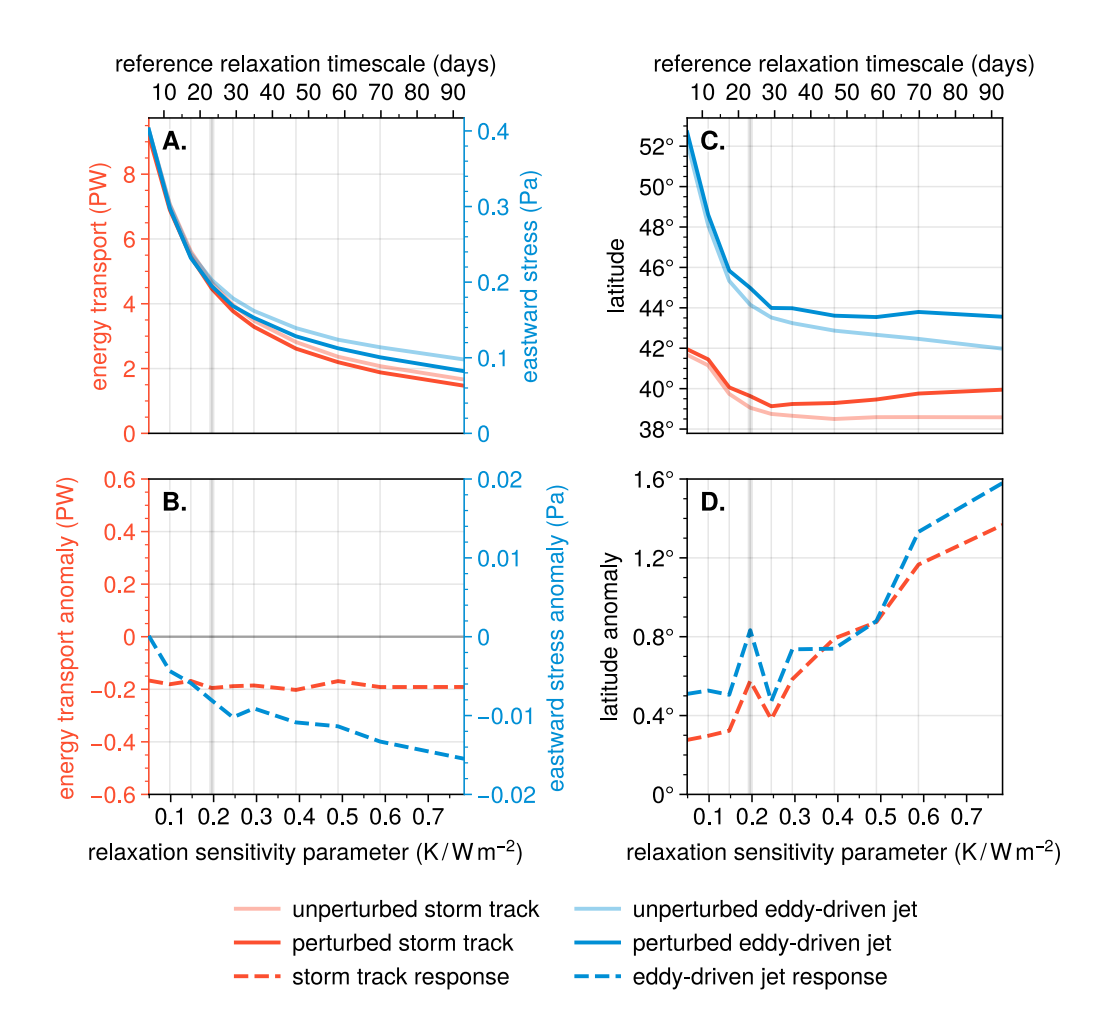


Fig. 10. Relaxation climate sensitivity and the extratropical circulation response to global warming. Steady-state extratropical circulation responses as a function of the relaxation sensitivity parameter s_{τ} (bottom x-axis) and the reference thermal relaxation timescale τ_0 (top x-axis). (A) The storm track intensity (solid red) and eddy-driven jet strength (solid blue) for the unperturbed control experiments (faded colors) and the perturbed global warming experiments (saturated colors). (B) The perturbed minus unperturbed storm track intensity (dashed red) and eddy-driven jet strength (dashed blue). (C, D) As in A, B, but for the latitudes and latitude shifts of the storm track (red) and eddy-driven jet (blue). The configurations we explicitly tested are indicated with vertical grid lines, and the Held and Suarez (1994) configuration is indicated with the thick vertical grid line. The storm track and eddy-driven jet are defined in Section 5.

independent of relaxation climate sensitivity and decoupled from the temperature response. This decoupling is consistent with the differing static energy diffusivities of climates with different relaxation climate sensitivities (Figure 5, B, solid and dashed medium gray lines).

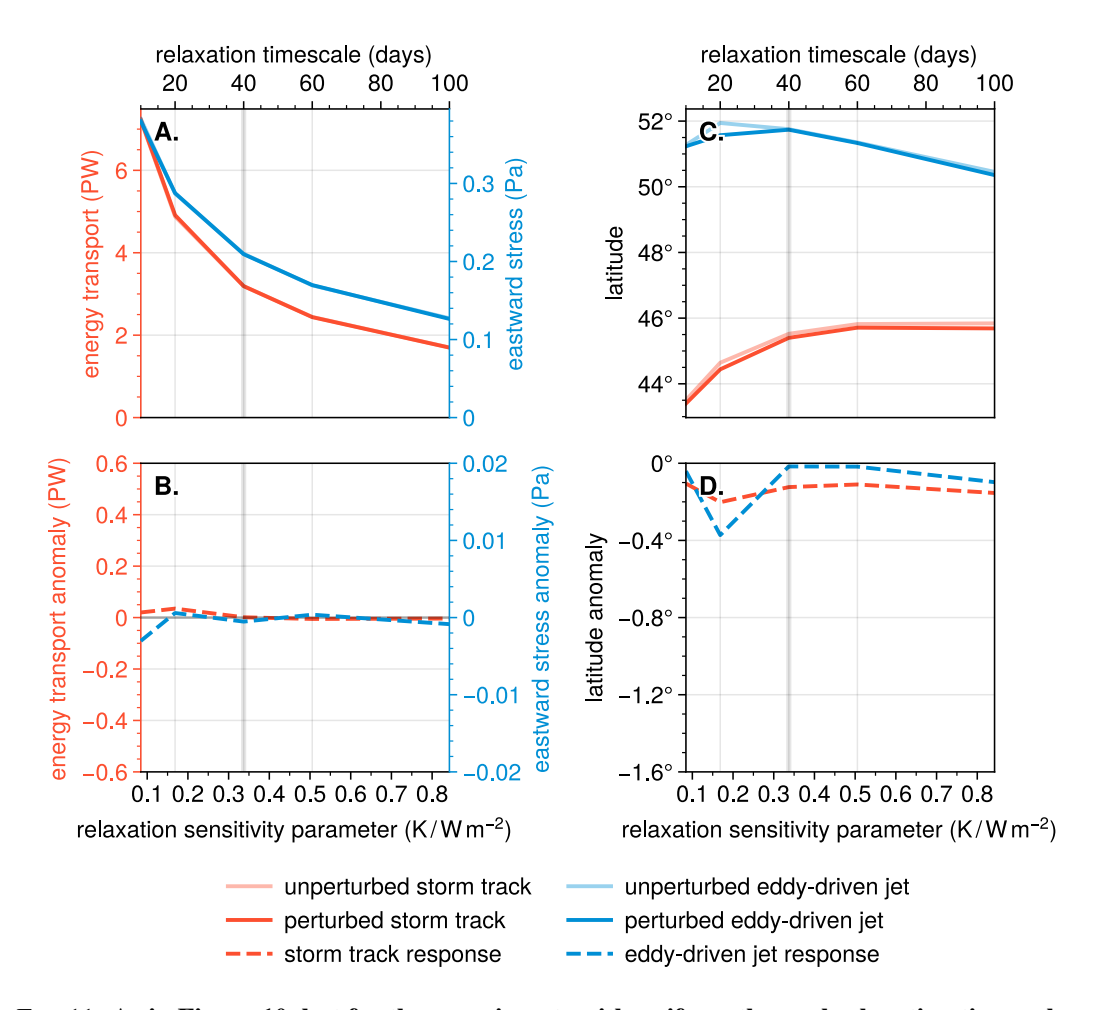


Fig. 11. As in Figure 10, but for the experiments with uniform thermal relaxation timescales.

The forcing perturbation *H* also leads to a weakening of the eddy-driven jet (Figure 10, A–B, blue lines), consistent with the strong coupling between eddy-driven jet strength and storm track intensity (Figure 5, C, red and blue lines). However, unlike the storm track response, the eddy-driven jet response is generally larger for configurations with higher relaxation climate sensitivity (Figure 10, B). This may come about because the eddy-driven jet strength is not energetically constrained, but rather determined by the structure of eddy momentum fluxes. These momentum fluxes reflect characteristics of wave propagation and dissipation, which itself depends on meridional and vertical temperature gradients. The larger eddy-driven jet response is then consistent with the larger temperature pattern response found under higher relaxation climate sensitivity (Figure 8, A–C, shading). Similarly, the absence of an eddy-driven jet response under spatially uniform relaxation feedback parameters (compare Figures 10 and 11, A–B, blue lines) is consistent with the absence

of a temperature pattern response under any corresponding relaxation climate sensitivity (Figure 9, A–C, shading).

In sum, Figures 7–11 highlight the key role of the relaxation climate sensitivity in determining not only the temperature response but also the large-scale circulation response to external forcing perturbations. Under a fixed spatial pattern of relaxation feedback parameters, the warming response pattern is larger for higher relaxation climate sensitivity, resulting in a larger zonal wind response and larger poleward shifts in the storm track and eddy-driven jet. By contrast, the thermal forcing response pattern is mainly independent of relaxation climate sensitivity, resulting in a constant reduction in storm track intensity. Importantly, the circulation response virtually disappears under spatially uniform relaxation feedback parameters. This highlights the critical roles of both the feedback parameters and the warming response pattern in guiding the circulation response to forcing perturbations.

7. Concluding remarks

The key results of this study are as follows.

- The thermal relaxation coefficient used with dynamical core models (i.e., the *relaxation feed-back parameter*) is analogous to the local climate feedback parameter, and the inverse average of the thermal relaxation coefficient (i.e., the *relaxation sensitivity parameter*) is analogous to the reference climate sensitivity parameter. Correspondingly, the warming response to forcing perturbations is proportional to the thermal relaxation timescale (Figure 1; Figure 7, B), and latitude-height patterns of relaxation coefficients that resemble clear-sky radiative kernels from more complex models lead to similar latitude-height patterns of warming (Figure 2; Figure 8, A–C). Dynamical core models are thus effective tools for studying relationships between climate sensitivity, climate feedbacks, and the large-scale circulation.
- In dynamical core models, lower relaxation climate sensitivities (i.e., shorter relaxation timescales) are associated with more vigorous large-scale circulations (Figure 4), including stronger and more poleward storm tracks and eddy-driven jets and increased thermal diffusivity (Figure 5). Differences in the large-scale circulation under different relaxation climate sensitivities are effectively characterized by energetic constraints: Lower relaxation climate sensitivity leads to stronger thermal forcing in the extratropics that must be balanced

by enhanced eddy static energy transport and thus stronger storm tracks in the steady-state average. This suggests that expected increases in equilibrium climate sensitivity under future warming scenarios (e.g., Senior and Mitchell 2000; Williams et al. 2008; Meraner et al. 2013) may further complicate a mechanistic understanding of the circulation response to warming.

- Under a horizontally uniform "global warming" forcing perturbation (Figure 3, C), lower relaxation climate sensitivity leads to a largely weaker large-scale circulation response (Figure 8), with less poleward displacement of the storm tracks and eddy-driven jets (Figure 10, C–D). The circulation response disappears if the perturbation experiment is repeated with a spatially uniform relaxation feedback parameter (compare Figures 8 and 9, D–F; Figures 10 and 11), suggesting that the circulation response to homogeneous forcing perturbations is dependent on spatial inhomogeneities in the local feedback parameter and the warming pattern resulting from those inhomogeneities.
- Under the same latitude-height pattern of relaxation feedback parameters (Figure 3, B), the relaxation climate sensitivity has relatively little effect on the magnitude of the storm track intensity response to forcing perturbations (Figure 10, A–B). This is because the eddy energy transport response is constrained by the energy budget response, which itself is the summation of 1) a constant forcing perturbation and 2) a mostly constant thermal forcing response arising from local temperature perturbations that are necessarily proportional to the local feedback parameters (Equation 3). The storm track intensity may thus have simpler constraints than most other aspects of the extratropical circulation.

Past dynamical core model studies of the circulation response to global warming have used localized heating terms to generate the warming patterns associated with spatially dependent climate feedback mechanisms (e.g., Butler et al. 2010; Mbengue and Schneider 2013; Lu et al. 2014; Sun et al. 2013). But the interpretability of these results is somewhat limited, since the pattern and magnitude of the real-world warming response is itself determined by the circulation (e.g., Davis and Birner 2022). We therefore suggest that future studies use a "relaxation timescale-aware" approach to simulating global warming in dynamical core models. By using relaxation timescales to model spatially dependent feedback mechanisms, the dynamics are given more freedom to determine the warming patterns ultimately generated by forcing perturbations.

It is important to emphasize that the latitude-height patterns of relaxation feedback parameters used in this study are highly idealized (Figure 2, D). Instead of matching the radiative feedback parameters from coupled GCMs (Equations A4 and A5), we scaled the idealized HS94 relaxation coefficients by constant factors. For greater consistency with more realistic estimates of the radiative feedback kernel and climate sensitivity parameter (Figure 2, C; Figure 1, red and blue lines), an alternative configuration might be obtained by 1) decreasing the depth of the boundary layer, 2) increasing the average thermal relaxation timescale, and 3) increasing the meridional equilibrium temperature gradient (to compensate for the effect of larger relaxation timescales on circulation intensity). Nevertheless, the unadjusted HS94 configuration was sufficient to reproduce the typical warming pattern generated by coupled GCMs with impressive fidelity (Figure 8, A–C). This suggests that the HS94 amplified boundary layer relaxation used in nearly all modern dynamical core model studies is as important to the maintenance of a realistic climate as it is to the realization of a realistic response to forcing perturbations.

The experimental setup described here could be used to assess the effects of individual feedback parameters on the large-scale circulation. This could be done by replacing the forcing perturbation H (Equation 5) with a coupled GCM estimate of the CO₂ forcing pattern, then matching the spatial pattern of the relaxation feedback parameter λ_{τ} to coupled GCM estimates of the air temperature, specific humidity and shortwave and longwave cloud feedback parameters (see Appendix A). Dynamical core models thereby provide the potential for useful future studies on the interactions between climate feedbacks and both the magnitude and uncertainty of the circulation response to global warming.

Acknowledgments. We thank the two anonymous reviewers and Pedram Hassanzadeh for their constructive and helpful comments on the paper. We also thank Isaac Held for his thoughtful editing and additional comments on the manuscript. This work was supported by the National Science Foundation Climate and Large-Scale Dynamics Program. We acknowledge the Geophysical Fluid Dynamics Laboratory (GFDL) for providing the general circulation model used in this study.

Data availability statement. The general circulation model used in this study is available in its original form at https://www.gfdl.noaa.gov/fms/, and with modifications for this study at https://github.com/lukelbd/gfdl-fms. The code used to conduct the experiments described in this study is available at https://github.com/lukelbd/drycore. The sources of

the climate sensitivity parameter and radiative feedback kernel estimates shown in Figures 1 and 2 are described in the main text.

APPENDIX

APPENDIX A

Climate sensitivity and climate feedback metrics

a. Global feedback parameters

Equation 3 demonstrates the analogy between the thermal relaxation coefficient τ^{-1} and the local climate feedback parameter λ . Using a procedure similar to Armour et al. (2012), we can average Equation 3 to obtain dynamical core-friendly expressions for the "effective" global feedback parameter and global climate sensitivity.

First, suppose we define the full-atmosphere climate sensitivity $\overline{\langle \Delta T \rangle}$ as the temperature response averaged over the entire atmosphere (where the single overbar denotes a horizontal average and the single angle brackets denote a vertical average). An expression for $\overline{\langle \Delta T \rangle}$ can be obtained by taking the horizontal average vertical integral of Equation 3 (where the double angle brackets denote a vertical integral):

$$\overline{\left\langle \left\langle -\frac{C}{\tau} \Delta T \right\rangle \right\rangle} = \overline{\left\langle \left\langle \lambda_{\tau} \Delta T \right\rangle \right\rangle} = \hat{\lambda}_{\tau} \overline{\left\langle \Delta T \right\rangle} = \overline{\left\langle \left\langle \Delta Q \right\rangle \right\rangle} = \overline{\left\langle \left\langle \Delta N \right\rangle \right\rangle} - \overline{\left\langle \left\langle H \right\rangle \right\rangle} \tag{A1}$$

In the context of the full-atmosphere response, the relaxation feedback parameter $\lambda_{\tau} \equiv -C/\tau$ represents the *local climate feedback parameter* and the response-weighted average $\hat{\lambda}_{\tau} \equiv \overline{\langle\langle \lambda_{\tau} \Delta T \rangle\rangle}/\overline{\langle \Delta T \rangle}$ represents the *effective global feedback parameter*. The global average vertical integral of the forcing perturbation H is analogous to the global average of the top-of-atmosphere radiative forcing perturbation from Equation 1.

Second, suppose we define the level-i climate sensitivity $\overline{\Delta T}_i$ as the global average temperature response at level i – say, the 1000 hPa pressure level. An expression for $\overline{\Delta T}_i$ can be obtained by regrouping the terms used to define the local feedback parameter in Equation A1 in an effort to

linearize the response around the temperature of level i:

$$\frac{\overline{\langle\langle\langle \lambda_{\tau} \Delta T \rangle\rangle\rangle}}{\Delta T_i} \Delta T_i = \overline{\lambda_{i\tau} \Delta T_i} = \hat{\lambda}_{i\tau} \overline{\Delta T}_i = \overline{\langle\langle\langle \Delta Q \rangle\rangle\rangle} = \overline{\langle\langle\langle \Delta N \rangle\rangle\rangle} - \overline{\langle\langle\langle H \rangle\rangle\rangle}$$
(A2)

In the context of the level-i response, the scaled relaxation feedback parameter $\lambda_{i\tau} \equiv \langle \langle \lambda_{\tau} \Delta T \rangle \rangle / \Delta T_i$ represents the *local climate feedback parameter* and the response-weighted average $\hat{\lambda}_{i\tau} \equiv \overline{\lambda_{i\tau} \Delta T_i} / \overline{\Delta T_i}$ represents the *effective global feedback parameter*. This effective global feedback parameter is similar to $\hat{\lambda}_{\tau}$ (Equation A1), except the associated local feedback parameter is weighted by the temperature response from a single level rather than all levels – analogous to a weighting by the surface temperature response ΔT_s .

Equations A1 and A2 represent dynamical core-equivalents of a global climate feedback analysis under spatially dependent feedbacks (e.g., Boer and Yu 2003a,b; Armour et al. 2012; Feldl and Roe 2013). They express the climate sensitivity in terms of the spatial pattern of the local feedbacks, the spatial pattern of the temperature response, and the global average of the forcing perturbation.

b. Radiative feedback kernels

In more complex models, the local climate feedback parameter λ is often broken down into the sum of component feedback parameters. These are the separate radiative responses to changes in air temperature, specific humidity, cloud properties, surface temperature, and surface albedo associated with the full response of the climate system to forcing perturbations (e.g., Hansen et al. 1985). Each component feedback parameter can be estimated as the product of a so-called *radiative feedback kernel* and a climate response term (e.g., Soden and Held 2006; Soden et al. 2008; Shell et al. 2008). For example, the component feedback parameter λ_T associated with changes in air temperature can be expressed as follows:

$$\lambda_T = \left\langle \left\langle \frac{\partial R}{\partial T} \frac{\Delta T}{\Delta T_s} \right\rangle \right\rangle = \left\langle \left\langle K_T \frac{\Delta T}{\Delta T_s} \right\rangle \right\rangle \tag{A3}$$

where R is the top-of-atmosphere radiative flux, T is the air temperature, T_s is the surface temperature, and $K_T \equiv \partial R/\partial T$ is the air temperature radiative kernel. A comparison of λ_T from Equation A3 with $\lambda_{i\tau}$ from Equation A2 reveals that the relaxation feedback parameter $\lambda_{\tau} \equiv -C/\tau$ is analogous to the air temperature radiative kernel K_T , with the level-i response ΔT_i standing in for the surface

response ΔT_s . This also follows from the analogy between the dynamical core thermal forcing response $\Delta Q = \lambda_{\tau} \Delta T$ (Equation 3) and the top-of-atmosphere radiative response ΔR (Equation 1), which itself implies that the partial derivative $\partial Q/\partial T = \lambda_{\tau}$ is analogous to $\partial R/\partial T = K_T$.

Similar to Equation A3, if the remaining thermodynamic properties can be expressed as a function of air temperature, then the local feedback parameter λ can be expressed in terms of a net radiative feedback kernel K:

$$\lambda = \left\langle \left\langle \frac{\mathrm{d}R}{\mathrm{d}T} \frac{\Delta T}{\Delta T_{\mathrm{s}}} \right\rangle \right\rangle = \left\langle \left\langle K \frac{\Delta T}{\Delta T_{\mathrm{s}}} \right\rangle \right\rangle \tag{A4}$$

where $K \equiv \mathrm{d}R/\mathrm{d}T$ is the total derivative of the radiative response with respect to air temperature (i.e., including attendant changes to e.g. moisture). Again comparing λ from Equation A4 with $\lambda_{i\tau}$ from Equation A2 and noting the analogy between $\mathrm{d}Q/\mathrm{d}T = \lambda_{\tau}$ and $\mathrm{d}R/\mathrm{d}T = K_T$ (Equation 2), λ_{τ} also appears to be analogous to the *net* radiative kernel K.

Equation A4 suggests that a variety of climate feedbacks might be "encoded" in a dynamical core model by appropriately scaling λ_{τ} . For example, consider the clear-sky radiative response to a forcing perturbation driven by changes to air temperature and specific humidity. If we suppose that specific humidity q always responds to changes in air temperature T according to the Clausius-Clapeyron relation (i.e., the relative humidity is fixed; e.g., Held and Soden 2006), then an estimate for the combined temperature-specific humidity feedback parameter can be obtained as follows:

$$\lambda_{T,q} = \left\langle \!\! \left(K_T \frac{\Delta T}{\Delta T_{\rm s}} + K_q \frac{\Delta q}{\Delta T_{\rm s}} \right) \!\! \right) \approx \left\langle \!\! \left(K_T \frac{\Delta T}{\Delta T_{\rm s}} + K_q \frac{\partial q}{\partial T} \frac{\Delta T}{\Delta T_{\rm s}} \right) \!\! \right) = \left\langle \!\! \left(K_{T,q} \frac{\Delta T}{\Delta T_{\rm s}} \right) \!\! \right)$$
(A5)

where K_T is the temperature radiative kernel, K_q is the specific humidity radiative kernel, $K_{T,q} \equiv K_T + K_q \partial q/\partial T$ is the combined temperature-specific humidity radiative kernel, and $\partial q/\partial T$ represents the Clausius-Clapeyron scaling. If the latitude-height structure of the relaxation feedback parameter λ_τ resembles the radiative kernel $K_{T,q}$, the climate feedback due to water vapor might be thought of as "encoded" in a dynamical core model. Figure 2 compares the spatial pattern of λ_τ under the HS94 configuration of a dynamical core model against the radiative kernel $K_{T,q}$ estimated from a reanalysis data set.

c. Relaxation climate sensitivity

In more complex models, the global feedback parameter associated with changes in air temperature is often broken down into two components: 1) a so-called Planck feedback parameter λ_P , associated with the isothermal component of the full temperature response; and 2) a lapse rate feedback parameter λ_L , associated with deviations from the isothermal response (e.g., Hartmann 2015). The climate sensitivity ΔT per unit radiative forcing H associated with the isothermal response is generally called the reference climate sensitivity parameter, equivalent to $s_0 = -1/\lambda_P$.

In a dynamical core model, s_0 can be obtained analytically by solving Equations A1 and A2 for $s_0 = \Delta T / \overline{\langle\langle H \rangle\rangle}$ under the assumption of an isothermal response and an energy imbalance of zero (note the same result is obtained using either Equation A1 or Equation A2). We call this the relaxation climate sensitivity parameter s_τ , defined as follows:

$$\hat{\lambda}_{\tau} \approx \overline{\langle \langle \lambda_{\tau} \rangle \rangle} = -\overline{\langle \langle \frac{C}{\tau} \rangle \rangle} = -\frac{C_0}{\tau_0}$$

$$s_{\tau} = -\frac{1}{\overline{\langle \langle \lambda_{\tau} \rangle \rangle}} = \frac{\tau_0}{C_0}$$
(A6)

where $\tau_0 \equiv 1/\overline{\langle 1/\tau \rangle}$ is the reference thermal relaxation timescale, $C_0 \equiv \langle C \rangle$ is the heat capacity of the full atmospheric column in J m⁻² K⁻¹, and the first line invokes the isothermal assumption (see Equation A1). Figures 4–6 use τ_0 and s_τ to characterize the climate sensitivity of each model configuration.

Likewise, we call the temperature response ΔT implied by the relaxation sensitivity parameter s_{τ} due to the forcing perturbation H the relaxation climate sensitivity ΔT_{τ} , defined as follows:

$$\Delta T_{\tau} = -\frac{\overline{\langle\langle H \rangle\rangle}}{\overline{\langle\langle \lambda_{\tau} \rangle\rangle}} = \overline{\langle\langle H \rangle\rangle} \frac{\tau_0}{C_0} \tag{A7}$$

The relaxation climate sensitivity represents the climate sensitivity of a dynamical core model under the assumption of an isothermal warming response (or spatially uniform feedback parameters; see Equation A1). Figure 7 compares the relaxation climate sensitivity ΔT_{τ} against empirical measures of the climate sensitivity ΔT obtained from simulations of a dynamical core model.

Interestingly, we can estimate the most physically realistic relaxation sensitivity parameter \hat{s}_{τ} for a given dynamical core model configuration using the physics of the Planck feedback parameter $\lambda_{\rm P}$. Under the HS94 configuration (see Appendix B), the average temperature over the entire atmosphere is around $\overline{\langle T \rangle} \approx 250\,{\rm K}$ – similar to the global average Earth emission temperature of $\overline{T}_{\rm e} \approx 255\,{\rm K}$. If we use $\overline{\langle T \rangle}$ as a stand-in for the emission temperature $\overline{T}_{\rm e}$, then our realistic relaxation sensitivity parameter is derived from the Stefan-Boltzmann Law as follows (e.g., Hartmann 2015):

$$\hat{s}_{\tau} = -\frac{1}{\lambda_{P}} = \left(\frac{\partial \left(\sigma \overline{T}_{e}^{4}\right)}{\partial \overline{T}_{e}}\right)^{-1} = \left(4\sigma \overline{T}_{e}^{3}\right)^{-1} \approx 0.28 \,\mathrm{K/W} \,\mathrm{m}^{-2} \tag{A8}$$

where σ is the Stefan-Boltzmann constant. Figure 1 compares the HS94 relaxation sensitivity parameter s_{τ} against the realistic relaxation sensitivity parameter \hat{s}_{τ} and a coupled climate model estimate of the reference sensitivity parameter s_0 .

APPENDIX B

Dynamical core model description

For the experiments described in the main text, we used the spectral dynamical core model from the Geophysical Fluid Dynamics Laboratory. We ran the model with a truncation level of 85 and with 60 vertical hybrid levels spaced according to the European Center for Medium-Range Weather Forecasts (ECMWF) "L60" specification (used by ECMWF to generate the ERA-Interim reanalysis product; Dee et al. 2011).

Each simulation was carried out with a simple perturbation from the standard HS94 model configuration. Under HS94, the thermal relaxation rate $Q = -C(T - T^e)/\tau$ is evaluated using the following analytic expressions for the equilibrium temperature T^e and the thermal relaxation timescale τ (see Figure 3, A–B):

$$T^{e} = \max \left\{ T_{\min}^{e}, \left(\overline{T}_{s}^{e} + \Delta_{h}^{e} \left(\frac{1}{3} - \sin^{2} \phi \right) - \Delta_{v}^{e} \cos^{2} \phi \log \left(\frac{p}{p_{0}} \right) \right) \left(\frac{p}{p_{0}} \right)^{\kappa} \right\}$$
 (B1)

$$\frac{1}{\tau} = \frac{1}{\tau_{\text{max}}} + \left(\frac{1}{\tau_{\text{min}}} - \frac{1}{\tau_{\text{max}}}\right) \max\left\{0, \frac{\sigma - \sigma_{\text{b}}}{1 - \sigma_{\text{b}}}\right\} \cos^{4}(\phi)$$
(B2)

Above, ϕ is latitude, p is pressure, and $\sigma \equiv p/p_s$ is the sigma height coordinate, where p_s is the instantaneous surface pressure; $\sigma_b = 0.7$ is the sigma coordinate representing the top of the boundary layer; $\tau_{\text{max}} = 40$ days is the maximum thermal relaxation timescale, realized everywhere above σ_b ; $\tau_{\text{min}} = 4$ days is the minimum thermal relaxation timescale, realized at the surface on the equator; $T_{\text{min}}^e = 200\,\text{K}$ is the isothermal stratospheric equilibrium temperature; $\overline{T}_s^e = 300\,\text{K}$ is the global average surface equilibrium temperature; $\Delta_h^e = 60\,\text{K}$ is the equator-pole equilibrium temperature difference at the surface; $\Delta_v^e = 10\,\text{K}$ controls the magnitude of the equilibrium static stability in the tropics; $p_0 \equiv 10^5\,\text{Pa}$ is the reference pressure; and $\kappa \equiv R_d/c_p$ is the Poisson constant, where R_d is the dry air gas constant and c_p is the specific heat at constant pressure.

Each simulation lasted 5500 days or 7500 days, with the first 500 days discarded to account for model spin-up. We compiled climatological averages from the remaining days. Since all of our forcing configurations are hemispherically symmetric, we use northern-southern hemisphere averages of the climatological averages to increase the effective sample size. For most of the simulations, we initialized the model with "cold starts" by imposing randomized small-amplitude vorticity perturbations on an isothermal initial state. However, the spin-up time for cold starts was often longer than 500 days for simulations with long thermal relaxation timescales and small meridional equilibrium temperature gradients. Therefore, we used "warm starts" for configurations with $\tau_{max} > 40$ days or $\Delta_h^e < 60\,K$ (their HS94 values). A "warm start" consisted of initializing the model with the final state from the preceding simulation in the corresponding experiment. For example, we began the $\tau_{max} = 100$ day simulation with the final timestep from the $\tau_{max} = 40$ day simulation, the τ_{max} = 200 day simulation with the final timestep from the τ_{max} = 100 day simulation, etc. This considerably reduced the spin-up period as diagnosed from time series of extratropical circulation metrics (not shown). The resulting steady-state climates were also no different from climates obtained with cold start initializations – the same steady-state solutions were just obtained more quickly. The simulations that required warm starts were also subject to long timescales of extratropical circulation variability. Therefore, to better resolve the steadystate responses to forcing perturbations, we ran the unperturbed and perturbed simulations with $\tau_{\text{max}} > 40$ days for an extra 2000 days (7500 days instead of 5500 days).

References

- Alexeev, V. A., P. L. Langen, and J. R. Bates, 2005: Polar amplification of surface warming on an aquaplanet in "ghost forcing" experiments without sea ice feedbacks. *Climate Dynamics*, **24** (7-8), 655–666, https://doi.org/10.1007/s00382-005-0018-3.
- Andrews, T., J. M. Gregory, and M. J. Webb, 2014: The Dependence of Radiative Forcing and Feedback on Evolving Patterns of Surface Temperature Change in Climate Models. *Journal of Climate*, **28** (**4**), 1630–1648, https://doi.org/10.1175/JCLI-D-14-00545.1.
- Andrews, T., J. M. Gregory, M. J. Webb, and K. E. Taylor, 2012: Forcing, feedbacks and climate sensitivity in CMIP5 coupled atmosphere-ocean climate models. *Geophysical Research Letters*, **39** (9), https://doi.org/10.1029/2012GL051607.
- Armour, K. C., C. M. Bitz, and G. H. Roe, 2012: Time-Varying Climate Sensitivity from Regional Feedbacks. *Journal of Climate*, **26** (**13**), 4518–4534, https://doi.org/10.1175/JCLI-D-12-00544. 1.
- Boer, G., and B. Yu, 2003a: Climate sensitivity and response. *Climate Dynamics*, **20** (**4**), 415–429, https://doi.org/10.1007/s00382-002-0283-3.
- Boer, G. J., and B. Yu, 2003b: Climate sensitivity and climate state. *Climate Dynamics*, **21** (2), 167–176, https://doi.org/10.1007/s00382-003-0323-7.
- Boljka, L., T. G. Shepherd, and M. Blackburn, 2018: On the Coupling between Barotropic and Baroclinic Modes of Extratropical Atmospheric Variability. *Journal of the Atmospheric Sciences*, **75** (6), 1853–1871, https://doi.org/10.1175/JAS-D-17-0370.1.
- Bony, S., and Coauthors, 2015: Clouds, circulation and climate sensitivity. *Nature Geoscience*, **8** (4), 261–268, https://doi.org/10.1038/ngeo2398.
- Butler, A. H., D. W. J. Thompson, and R. Heikes, 2010: The Steady-State Atmospheric Circulation Response to Climate Change–like Thermal Forcings in a Simple General Circulation Model. *Journal of Climate*, **23** (**13**), 3474–3496, https://doi.org/10.1175/2010JCLI3228.1.
- Ceppi, P., and D. L. Hartmann, 2016: Clouds and the Atmospheric Circulation Response to Warming. *Journal of Climate*, **29** (2), 783–799, https://doi.org/10.1175/JCLI-D-15-0394.1.

- Chen, G., I. M. Held, and W. A. Robinson, 2007: Sensitivity of the Latitude of the Surface Westerlies to Surface Friction. *Journal of the Atmospheric Sciences*, **64** (**8**), 2899–2915, https://doi.org/10.1175/JAS3995.1.
- Chen, G., P. Zhang, and J. Lu, 2020: Sensitivity of the Latitude of the Westerly Jet Stream to Climate Forcing. *Geophysical Research Letters*, **47** (**4**), e2019GL086563, https://doi.org/10.1029/2019GL086563.
- Crook, J. A., P. M. Forster, and N. Stuber, 2011: Spatial Patterns of Modeled Climate Feedback and Contributions to Temperature Response and Polar Amplification. *Journal of Climate*, **24** (**14**), 3575–3592, https://doi.org/10.1175/2011JCLI3863.1.
- Davis, N. A., and T. Birner, 2022: Eddy-mediated Hadley cell expansion due to axisymmetric angular momentum adjustment to greenhouse gas forcings. *Journal of the Atmospheric Sciences*, -1 (aop), https://doi.org/10.1175/JAS-D-20-0149.1.
- Dee, D. P., and Coauthors, 2011: The ERA-Interim reanalysis: Configuration and performance of the data assimilation system. *Quarterly Journal of the Royal Meteorological Society*, **137** (**656**), 553–597, https://doi.org/10.1002/qj.828.
- Dong, Y., K. C. Armour, M. D. Zelinka, C. Proistosescu, D. S. Battisti, C. Zhou, and T. Andrews, 2020: Intermodel Spread in the Pattern Effect and Its Contribution to Climate Sensitivity in CMIP5 and CMIP6 Models. *Journal of Climate*, **33** (**18**), 7755–7775, https://doi.org/10.1175/JCLI-D-19-1011.1.
- Feldl, N., and G. H. Roe, 2013: Four perspectives on climate feedbacks. *Geophysical Research Letters*, **40** (**15**), 4007–4011, https://doi.org/10.1002/grl.50711.
- Hall, A., P. Cox, C. Huntingford, and S. Klein, 2019: Progressing emergent constraints on future climate change. *Nature Climate Change*, **9** (4), 269–278, https://doi.org/10.1038/s41558-019-0436-6.
- Hansen, J., G. Russell, A. Lacis, I. Fung, D. Rind, and P. Stone, 1985: Climate Response Times: Dependence on Climate Sensitivity and Ocean Mixing. *Science*, **229** (**4716**), 857–859.
- Hartmann, D. L., 2015: Global Physical Climatology. 2nd ed., Elsevier Science.

- Held, I. M., and B. J. Soden, 2000: Water Vapor Feedback and Global Warming. *Annual Review of Energy and the Environment*, **25** (1), 441–475, https://doi.org/10.1146/annurev.energy.25.1.441.
- Held, I. M., and B. J. Soden, 2006: Robust Responses of the Hydrological Cycle to Global Warming. *Journal of Climate*, **19** (**21**), 5686–5699, https://doi.org/10.1175/JCLI3990.1.
- Held, I. M., and M. J. Suarez, 1994: A Proposal for the Intercomparison of the Dynamical Cores of Atmospheric General Circulation Models. *Bulletin of the American Meteorological Society*, **75** (**10**), 1825–1830, https://doi.org/10.1175/1520-0477(1994)075<1825:APFTIO>2.0.CO;2.
- Holland, M. M., and C. M. Bitz, 2003: Polar amplification of climate change in coupled models. *Climate Dynamics*, **21** (**3**), 221–232, https://doi.org/10.1007/s00382-003-0332-6.
- Huang, Y., 2022: ERA-interim reanalysis based radiative kernels. Mendeley Data, https://doi.org/ 10.17632/3drx8fmmz9.1.
- Huang, Y., Y. Xia, and X. Tan, 2017: On the pattern of CO2 radiative forcing and poleward energy transport. *Journal of Geophysical Research: Atmospheres*, **122** (**20**), 10,578–10,593, https://doi.org/10.1002/2017JD027221.
- Klein, S. A., and A. Hall, 2015: Emergent Constraints for Cloud Feedbacks. *Current Climate Change Reports*, **1** (**4**), 276–287, https://doi.org/10.1007/s40641-015-0027-1.
- Kushner, P. J., and L. M. Polvani, 2004: Stratosphere–Troposphere Coupling in a Relatively Simple AGCM: The Role of Eddies. *Journal of Climate*, **17** (3), 629–639, https://doi.org/10.1175/1520-0442(2004)017<0629:SCIARS>2.0.CO;2.
- Kushner, P. J., and L. M. Polvani, 2006: Stratosphere–Troposphere Coupling in a Relatively Simple AGCM: Impact of the Seasonal Cycle. *Journal of Climate*, **19** (**21**), 5721–5727, https://doi.org/10.1175/JCLI4007.1.
- Li, Y., D. W. J. Thompson, S. Bony, and T. M. Merlis, 2019: Thermodynamic Control on the Poleward Shift of the Extratropical Jet in Climate Change Simulations: The Role of Rising High Clouds and Their Radiative Effects. *Journal of Climate*, **32** (3), 917–934, https://doi.org/10.1175/JCLI-D-18-0417.1.

- Lu, J., L. Sun, Y. Wu, and G. Chen, 2014: The Role of Subtropical Irreversible PV Mixing in the Zonal Mean Circulation Response to Global Warming–Like Thermal Forcing. *Journal of Climate*, **27** (6), 2297–2316, https://doi.org/10.1175/JCLI-D-13-00372.1.
- Mbengue, C., and T. Schneider, 2013: Storm Track Shifts under Climate Change: What Can Be Learned from Large-Scale Dry Dynamics. *Journal of Climate*, **26** (**24**), 9923–9930, https://doi.org/10.1175/JCLI-D-13-00404.1.
- Meraner, K., T. Mauritsen, and A. Voigt, 2013: Robust increase in equilibrium climate sensitivity under global warming. *Geophysical Research Letters*, **40** (**22**), 5944–5948, https://doi.org/10. 1002/2013GL058118.
- O'Gorman, P. A., and C. J. Muller, 2010: How closely do changes in surface and column water vapor follow Clausius–Clapeyron scaling in climate change simulations? *Environmental Research Letters*, **5** (2), 025 207, https://doi.org/10.1088/1748-9326/5/2/025207.
- Pithan, F., and T. Mauritsen, 2014: Arctic amplification dominated by temperature feedbacks in contemporary climate models. *Nature Geoscience*, **7** (**3**), 181–184, https://doi.org/10.1038/ngeo2071.
- Senior, C. A., and J. F. B. Mitchell, 2000: The time-dependence of climate sensitivity. *Geophysical Research Letters*, **27** (**17**), 2685–2688, https://doi.org/10.1029/2000GL011373.
- Shaw, T. A., 2019: Mechanisms of Future Predicted Changes in the Zonal Mean Mid-Latitude Circulation. *Current Climate Change Reports*, **5** (**4**), 345–357, https://doi.org/10.1007/s40641-019-00145-8.
- Shaw, T. A., P. Barpanda, and A. Donohoe, 2018: A Moist Static Energy Framework for Zonal-Mean Storm-Track Intensity. *Journal of the Atmospheric Sciences*, **75** (6), 1979–1994, https://doi.org/10.1175/JAS-D-17-0183.1.
- Shaw, T. A., and Coauthors, 2016: Storm track processes and the opposing influences of climate change. *Nature Geoscience*, **9** (**9**), 656–664, https://doi.org/10.1038/ngeo2783.
- Shell, K. M., J. T. Kiehl, and C. A. Shields, 2008: Using the Radiative Kernel Technique to Calculate Climate Feedbacks in NCAR's Community Atmospheric Model. *Journal of Climate*, **21** (**10**), 2269–2282, https://doi.org/10.1175/2007JCLI2044.1.

- Shepherd, T. G., 2014: Atmospheric circulation as a source of uncertainty in climate change projections. *Nature Geoscience*, **7** (**10**), 703–708, https://doi.org/10.1038/ngeo2253.
- Soden, B. J., and I. M. Held, 2006: An Assessment of Climate Feedbacks in Coupled Ocean–Atmosphere Models. *Journal of Climate*, **19** (**14**), 3354–3360, https://doi.org/10.1175/JCLI3799.1.
- Soden, B. J., I. M. Held, R. Colman, K. M. Shell, J. T. Kiehl, and C. A. Shields, 2008: Quantifying Climate Feedbacks Using Radiative Kernels. *Journal of Climate*, **21** (**14**), 3504–3520, https://doi.org/10.1175/2007JCLI2110.1.
- Sun, L., G. Chen, and J. Lu, 2013: Sensitivities and Mechanisms of the Zonal Mean Atmospheric Circulation Response to Tropical Warming. *Journal of the Atmospheric Sciences*, **70** (**8**), 2487–2504, https://doi.org/10.1175/JAS-D-12-0298.1.
- Voigt, A., and T. A. Shaw, 2015: Circulation response to warming shaped by radiative changes of clouds and water vapour. *Nature Geoscience*, **8** (2), 102–106, https://doi.org/10.1038/ngeo2345.
- Williams, K. D., W. J. Ingram, and J. M. Gregory, 2008: Time Variation of Effective Climate Sensitivity in GCMs. *Journal of Climate*, **21** (**19**), 5076–5090, https://doi.org/10.1175/2008JCLI2371.1.
- Zelinka, M., 2021: Mzelinka/cmip56_forcing_feedback_ecs: Aug 16, 2021 Release. Zenodo, https://doi.org/10.5281/zenodo.5206851.
- Zelinka, M. D., T. A. Myers, D. T. McCoy, S. Po-Chedley, P. M. Caldwell, P. Ceppi, S. A. Klein, and K. E. Taylor, 2020: Causes of Higher Climate Sensitivity in CMIP6 Models. *Geophysical Research Letters*, **47** (1), e2019GL085782, https://doi.org/10.1029/2019GL085782.